SYNTHESIS AND MESOMORPHIC PROPERTIES OF SYMMETRIC AND NON-SYMMETRIC MULTI-FUNCTIONALIZED OLIGOMERS

by

HNG TIANG CHUAN

Thesis submitted in fulfillment of the requirements
for the degree of
Doctor of Philosophy

February 2009

ACKNOWLEDGEMENT

I wish to take this opportunity to thank my main supervisor, Professor Yeap Guan Yeow for his teaching and attention to my research throughout the period of my candidature. Also, I would like to express my appreciation to my co-supervisor, Professor Wan Ahmad Kamil Mahmood for giving me advice and assistance generously. I wish to thank the Dean and the staff of School of Chemical Sciences for providing me with the research facilities. My gratitude also goes to the Dean of Institute of Postgraduate Studies for giving me a chance to enroll as a PhD student at Universiti Sains Malaysia.

I would like to express my sincere appreciation to Professor Masato M. Ito of Soka University, Japan, Associate Professor Daisuke Takeuchi from Tokyo Institute of Technology, Japan and Professor Ewa Gorecka from Warsaw University, Poland for the assistance in several analyses on my liquid crystal samples. I wish to thank Professor Corrie T. Imrie of University of Aberdeen, Scotland, who is also my field supervisor, for sharing his expertise in liquid crystal research with me. I am also grateful to my laboratory mates for sharing their knowledge with me and providing me with great assistance in many aspects at the workplace.

To my family members and friends, I wish to convey my best regards and gratitude for their support all this while.

TABLE OF CONTENTS

ACKNOWLEDGEMENT ii

TABLE OF CONTENTS iii

LIST OF TABLES ix

LIST OF FIGURES xvi

ABSTRAK xxxii

ABSTRACT xxxiv

1.0 INTRODUCTION

1.1 Liquid crystals: History 1

1.2 Liquid crystals: Concept 1

1.3 Mesophases 2

- 1.3.1 Nematic phase 2
  - 1.3.1.1 Chiral nematic phase 3
- 1.3.2 Smectic phase 4
  - 1.3.2.1 Non-chiral smectic phase 4
  - 1.3.2.2 Chiral smectic phase 8
  - 1.3.2.3 Unidentified smectic phase 9
- 1.3.3 Blue phase 9

1.4 Mesogen 10

- 1.4.1 Calamitic mesogens 10
- 1.4.2 Discotic mesogens 11
- 1.4.3 Banana-shaped mesogens 12
- 1.4.4 Laterally branched mesogens 12
- 1.4.5 Oligomeric mesogens 13

1.5 Structure-property relationship of liquid crystals 15

1.5.1 Structure-property relationship of liquid crystal oligomers 16

1.5.1.1 The influence of spacer length and parity on the liquid crystalline properties of oligomers 16

1.5.1.2 The influence of unlike cores and non-symmetric structures on the liquid crystalline properties of oligomers 17

1.5.2 Chirality effect on liquid crystalline properties 17

1.6 Application of liquid crystals 18

1.7 Objectives of the research 19

2.0 EXPERIMENTAL

2.1 Chemicals 21

2.2 Equipment 22

2.3 Synthesis and characterization 23

2.3.1 First series α-(4-Benzylidene-substituted-aniline-4’-oxy)-ω-[2-methylbutyl-4’-(4”-phenyl)benzoateoxy]alkanes, **4a**-**4j** 24

2.3.1.1 Synthesis of (*RS*)-2-methylbutyl-4’-(4”-hydroxyphenyl)benzoate, **1** 24

2.3.1.2 Synthesis of 4-hydroxy-4’-benzylidene-substituted-anilines, **2a**-**2e** 24

2.3.1.3 Synthesis of 4-(*n*-bromoalkyloxy)-4’-benzylidene-substituted-anilines, **3a**-**3j** 25

2.3.1.4 Synthesis of α-(4-benzylideneaniline-4’-oxy)-ω-[2-methylbutyl-4’-(4”-phenyl)benzoateoxy]alkanes, **4a**-**4j** 27

2.3.2 Second series α-(4-Benzylidenechloroaniline-4’-oxy)-ω-[4-(thiophene-2-carboxyl)-benzylideneaniline-4’-oxy]alkanes, **9a**-**9h** 28

2.3.2.1 Synthesis of 4-formylphenyl thiophene-2-carboxylate, **5** 29

2.3.2.2 Synthesis of 4-(thiophene-2-carboxyl)benzylidene-4’-hydroxyaniline, **6** 30

2.3.2.3 Synthesis of 4-hydroxy-4’-benzylidenechloroaniline, **7** and 4-(*n*-bromoalkyloxy)-4’-benzylidenechloroanilines, **8a**-**8h** 30

2.3.2.4 Synthesis of α-(4-benzylidenechloroaniline-4’-oxy)-ω-[4-(thiophene-2-carboxyl)benzylideneaniline-4’-oxy]alkanes **9a**-**9h** 31

2.3.3 Third, fourth and fifth series 4,4’-Bis{ω-[2-methylbutyl-4’-(4”-phenyl)benzoateoxy]alkyloxy-benzylidene}-1,4-diaminobenzenes, **13a**-**13h**, 4,4’-bis{ω-[2-methylbutyl-4’-(4”-phenyl)benzoateoxy]-3-methoxy-4-alkyloxy-benzylidene}-1,4-diaminobenzenes, **16a**-**16h** and 4,4’-bis{ω-[2-methylbutyl-4’-(4”-phenyl)benzoateoxy]-3-bromo-4-alkyloxy-benzylidene}-1,4-diaminobenzenes, **19a**-**19h** 32

2.3.3.1 Synthesis of (*S*)-(-)-2-methylbutyl-4’-(4”-hydroxyphenyl)-benzoate, **10** 32

2.3.3.2 Synthesis of 4,4’-bis(4-hydroxybenzylidene)-1,4-diaminobenzene, **11**, 4,4’-bis(3-methoxy-4-hydroxy-benzylidene)-1,4-diaminobenzene, **14** and 4,4’-bis(3-bromo-4-hydroxybenzylidene)-1,4-diaminobenzene, **17** 34

2.3.3.3 Synthesis of 4,4’-bis[4-(*n*-bromoalkyloxy)benzylidene]-1,4-diaminobenzenes, **12a**-**12h**, 4,4’-bis[3-methoxy-4-(*n*-bromoalkyloxy)benzylidene]-1,4-diaminobenzenes, **15a**-**15h** and 4,4’-bis[3-bromo-4-(*n*-bromoalkyloxy)benzylidene]-1,4-diaminobenzenes, **18a**-**18h** 34

2.3.3.4 Synthesis of 4,4’-bis{ω-[2-methylbutyl-4’-(4”-phenyl)-benzoateoxy]alkyloxybenzylidene}-1,4-diaminobenzenes, **13a**-**13h**, 4,4’-bis{ω-[2-methylbutyl-4’-(4”-phenyl)-benzoateoxy]-3-methoxy-4-alkyloxybenzylidene}-1,4-diaminobenzenes, **16a**-**16h** and 4,4’-bis{ω-[2-methylbutyl-4’-(4”-phenyl)benzoateoxy]-3-bromo-4-alkyloxybenzylidene}-1,4-diaminobenzenes, **19a**-**19h** 35

2.3.4 Sixth series 4-Ethyl- and 4-fluoroanilinebenzylidene-2’,4’-oxybis(4”-halogeno-anilinebenzylidene-4”’-oxy)alkanes, **25a**-**25d** and **26a**-**26d** 38

2.3.4.1 Synthesis of 4-hydroxy-4’-benzylidene-substituted-anilines, **22a** and **22b** 39

2.3.4.2 Synthesis of 4-(*n*-bromoalkyloxy)-4’-benzylidene-substituted-anilines, **23a**-**23d** 39

2.3.4.3 Synthesis of benzyl-2,4-oxybis(4’-halogenoanilinebenzylidene-4”-oxy)alkane aldehydes, **24a**-**24d** 39

2.3.4.4 Synthesis of 4-ethyl- and 4-fluoroanilinebenzylidene-2’,4’-oxy-bis(4”-halogenoanilinebenzylidene-4”’-oxy)alkanes, **25a-25d** and **26a-26d** 40

3.0 RESULTS AND DISCUSSION FOR α-(4-BENZYLIDENE-SUBSTITUTED-ANILINE-4’-OXY)- ω-[2-METHYLBUTYL-4’-(4”-PHENYL)BENZOATEOXY]ALKANES

3.1 Physical characterization 42

3.1.1 (*RS*)-2-methylbutyl-4’-(4”-hydroxyphenyl)benzoate, **1** 42

3.1.2 4-Hydroxy-4’-benzylidene-substituted-anilines, **2a**-**2e** 50

3.1.3 4-(*n*-Bromoalkyloxy)-4’-benzylidene-substituted-anilines, **3a**-**3j** 60

3.1.4 α-(4-Benzylidene-substituted-aniline-4’-oxy)-ω-[2-methylbutyl-4’-(4”-phenyl)benzoateoxy]alkanes, **4a**-**4j** 72

3.2 Mesomorphic (liquid crystalline) properties 108

4.0 RESULTS AND DISCUSSION FOR α-(4-BENZYLIDENECHLORO-ANILINE-4’-OXY)-ω-[4-(THIOPHENE-2-CARBOXYL)-BENZYLIDENEANILINE-4’-OXY]ALKANES

4.1 Physical characterization 118

4.1.1 4-Formylphenyl thiophene-2-carboxylate, **5** 118

4.1.2 4-(Thiophene-2-carboxyl)benzylidene-4’-hydroxyaniline, **6** 124

4.1.3 4-Hydroxy-4’-benzylidenechloroaniline, **7** and 4-(*n*-bromoalkyloxy)-4’-benzylidenechloroanilines, **8a**-**8h** 130

4.1.4 α-(4-Benzylidenechloroaniline-4’-oxy)-ω-[4-(thiophene-2-carboxyl)-benzylideneaniline-4’-oxy]alkanes, **9a**-**9h** 136

4.2 Mesomorphic (liquid crystalline) properties 157

5.0 RESULTS AND DISCUSSION FOR 4,4’-BIS{ω-[2-METHYLBUTYL-4’-(4”-PHENYL)BENZOATEOXY]ALKYLOXYBENZYLIDENE}-1,4-DIAMINOBENZENES

5.1 Physical characterization 164

5.1.1 (*S*)-(-)-2-Methylbutyl-4’-(4”-hydroxyphenyl)benzoate, **10** 164

5.1.2 4,4’-Bis(4-hydroxybenzylidene)-1,4-diaminobenzene, **11** 169

5.1.3 4,4’-Bis[4-(*n*-bromoalkyloxy)benzylidene]-1,4-diaminobenzenes, **12a**-**12h** 172

5.1.4 4,4’-Bis{ω-[2-methylbutyl-4’-(4”-phenyl)benzoateoxy]alkyloxybenzylidene}-1,4-diaminobenzenes, **13a**-**13h** 180

5.2 Mesomorphic (liquid crystalline) properties 212

6.0 RESULTS AND DISCUSSION FOR 4,4’-BIS{ω-[2-METHYLBUTYL-4’-(4”-PHENYL)BENZOATEOXY]-3-METHOXY-4-ALKYLOXY-BENZYLIDENE}-1,4-DIAMINOBENZENES

6.1 Physical characterization 226

6.1.1 4,4’-Bis(3-methoxy-4-hydroxybenzylidene)-1,4-diaminobenzene, **14** 226

6.1.2 4,4’-Bis[3-methoxy-4-(*n*-bromoalkyloxy)benzylidene]-1,4-diaminobenzenes, **15a**-**15h** 230

6.1.3 4,4’-Bis{ω-[2-methylbutyl-4’-(4”-phenyl)benzoateoxy]-3-methoxy-4-alkyloxybenzylidene}-1,4-diaminobenzenes, **16a**-**16h** 238

6.2 Mesomorphic (liquid crystalline) properties 270

7.0 RESULTS AND DISCUSSION FOR 4,4’-BIS{ω-[2-METHYLBUTYL-4’-(4”-PHENYL)BENZOATEOXY]3-BROMO-4-ALKYLOXY-BENZYLIDENE}-1,4-DIAMINOBENZENES

7.1 Physical characterization 274

7.1.1 4,4’-Bis(3-bromo-4-hydroxybenzylidene)-1,4-diaminobenzene, **17** 274

7.1.2 4,4’-Bis[3-bromo-4-(*n*-bromoalkyloxy)benzylidene]-1,4-diaminobenzenes, **18a**-**18h** 277

7.1.3 4,4’-Bis{ω-[2-methylbutyl-4’-(4”-phenyl)benzoateoxy]-3-bromo-4-alkyloxybenzylidene}-1,4-diaminobenzenes, **19a**-**19h** 285

7.2 Mesomorphic (liquid crystalline) properties 317

8.0 RESULTS AND DISCUSSION FOR 4-ETHYL- AND 4-FLUORO-ANILINEBENZYLIDENE-2’,4’-OXYBIS(4”-HALOGENOANILINE-BENZYLIDENE-4”’-OXY)ALKANES

8.1 Physical characterization 325

8.1.1 4-Hydroxy-4’-benzylidene-substituted-anilines, **22a** and **22b** 325

8.1.2 4-(*n*-Bromoalkyloxy)-4’-benzylidene-substituted-anilines, **23a**-**23d** 328

8.1.3 Benzyl-2,4-oxybis(4’-halogenoanilinebenzylidene-4”-oxy)alkane aldehydes, **24a**-**24d** 335

8.1.4 4-Ethyl- and 4-fluoroanilinebenzylidene-2’,4’-oxybis(4”-halogenoanilinebenzylidene-4”’-oxy)alkanes, **25a**-**25d** and **26a**-**26d** 342

8.2 Mesomorphic (liquid crystalline) properties 378

9.0 CONCLUSIONS 389

REFERENCES 393

APPENDICES

Appendix A: International publications

Appendix B: Papers presented in international or regional conference / seminar

LIST OF TABLES

Table 2.1 List of chemicals used for the syntheses and respective assays 21

Table 2.2 General molecular formula and amounts of corresponding anilines for the syntheses of compounds **2a-2e** 25

Table 2.3 Amounts of compounds **2a-2e** and corresponding α,ω-dibromoalkanes for the syntheses of compounds **3a-3j** 27

Table 2.4 Amounts of compounds **3a-3j** for the syntheses of compounds **4a-4j** 28

Table 2.5 Amounts of corresponding α,ω-dibromoalkanes for the syntheses of compounds **8a-8h** 30

Table 2.6 Amounts of compounds **8a-8h** for the syntheses of compounds **9a-9h** 31

Table 2.7 Amounts of corresponding α,ω-dibromoalkanes for the syntheses of compounds **12a-12h**, **15a-15h** and **18a-18h** 35

Table 2.8 Amounts of compounds **10** and **12a-12h** for the syntheses of compounds **13a-13h** 36

Table 2.9 Amounts of compounds **10** and **15a-15h** for the syntheses of compounds **16a-16h** 37

Table 2.10 Amounts of compounds **10** and **18a-18h** for the syntheses of compounds **19a-19h** 37

Table 2.11 Amounts of compounds **22a**, **22b** and corresponding α,ω-dibromoalkanes for the syntheses of compounds **23a-23d** 39

Table 2.12 Amounts of compounds **23a-23d** for the syntheses of compounds **24a-24d** 40

Table 2.13 Amounts of compounds **24a-24d**, the general molecular formula and amounts of corresponding anilines for the syntheses of compounds **25a-25d** 41

Table 3.1 C and H microanalytical data of compound **1** 44

Table 3.2 Selected FT-IR absorption frequency (υ / cm^{-1}) of compound **1** 44

Table 3.3 List of ^{1}H-NMR chemical shifts (δ / ppm), multiplicity, number of protons and associated functional groups of compound **1** 47

Table 3.4 C, H and N microanalytical data of compounds **2a-2e** 52

Table 3.5 Selected FT-IR absorption frequency (υ / cm^{-1}) of compounds **2a-2e** 53

Table 3.6 List of ^{1}H-NMR chemical shifts (δ / ppm), multiplicity, number of protons and associated functional groups of compounds **2a**-**2e** 60

Table 3.7 Yields (%) of compounds **3a**-**3j** 62

Table 3.8 C, H and N microanalytical data of compounds **3a**-**3j** 62

Table 3.9 Selected FT-IR absorption frequency (υ / cm^{-1}) of compounds **3a**-**3j** 66

Table 3.10 List of ^{1}H-NMR chemical shifts (δ / ppm), multiplicity, number of protons and associated functional groups of compounds **3a**-**3j** 71

Table 3.11 Yields (%) of compounds **4a**-**4j** 73

Table 3.12 C, H and N microanalytical data of compounds **4a**-**4j** 73

Table 3.13 Selected FT-IR absorption frequency (υ / cm^{-1}) of compounds **4a**-**4j** 75

Table 3.14 Chemical shifts (δ / ppm) for the selected protons of compound **4b** 81

Table 3.15 Chemical shifts (δ / ppm) for the selected carbons and ^{1}H-^{13}C HMQC and HMBC correlations of compound **4b** 91

Table 3.16 Chemical shifts (δ / ppm) for the quaternary carbons of compound **4b** 92

Table 3.17 Chemical shifts (δ / ppm) for the selected protons of compound **4d** 96

Table 3.18 Chemical shifts (δ / ppm) for the selected carbons and ^{1}H-^{13}C HMQC and HMBC correlations of compound **4d** 104

Table 3.19 Chemical shifts (δ / ppm) for the quaternary carbons of compound **4d** 105

Table 3.20 Chemical shifts (δ / ppm) for the selected protons of compounds **4a**, **4c** and **4e**-**4j** 106

Table 3.21 Chemical shifts (δ / ppm) for the selected carbons of compounds **4a**, **4c** and **4e** 107

Table 3.22 Chemical shifts (δ / ppm) for the selected carbons of compounds **4f**-**4j** 108

Table 3.23 The phase transition temperatures (°C), associated enthalpy changes (kJmol^{-1}) and nematic-isotropic entropy changes of compounds **4a**-**4j**. Virtual transition temperatures obtained by extrapolation of phase diagrams are given in [ ]. Only the highest melting points are listed. (● = enantiotropic phase, ○ = monotropic phase, Cr = crystal, SmA$_c$ = intercalated SmA, N = nematic, I = isotropic) 109

Table 4.1 C and H microanalytical data of compound **5** 120

Table 4.2 Selected FT-IR absorption frequency (υ / cm^{-1}) of compound **5** 121

Table 4.3 List of ^{1}H-NMR chemical shifts (δ / ppm), multiplicity, number of protons and associated functional groups of compound **5** 121

Table 4.4 C, H and N microanalytical data of compound **6** 125

Table 4.5 Selected FT-IR absorption frequency (υ / cm^{-1}) of compound **6** 126

Table 4.6 List of ^{1}H-NMR chemical shifts (δ / ppm), multiplicity, number of protons and associated functional groups of compound **6** 127

Table 4.7 Yields (%) of compounds **8a-8h** 131

Table 4.8 C, H and N microanalytical data of compounds **8a-8h** 131

Table 4.9 Selected FT-IR absorption frequency (υ / cm^{-1}) of compounds **8a-8h** 133

Table 4.10 List of ^{1}H-NMR chemical shifts (δ / ppm), multiplicity, number of protons and associated functional groups of compounds **8a-8h** 135

Table 4.11 Yields (%) of compounds **9a-9h** 137

Table 4.12 C, H and N microanalytical data of compounds **9a-9h** 137

Table 4.13 Selected FT-IR absorption frequency (υ / cm^{-1}) of compounds **9a-9h** 138

Table 4.14 Chemical shifts (δ / ppm) for the selected protons of compound **9c** 142

Table 4.15 Chemical shifts (δ / ppm) for the selected carbons and ^{1}H-^{13}C HMQC and HMBC correlations of compound **9c** 154

Table 4.16 Chemical shifts (δ / ppm) for the quaternary carbons of compound **9c** 155

Table 4.17 Chemical shifts (δ / ppm) for the selected protons of compounds **9a**, **9b** and **9d-9h** 155

Table 4.18 Chemical shifts (δ / ppm) for the selected carbons of compounds **9a**, **9b**, **9d** and **9e** 156

Table 4.19 Chemical shifts (δ / ppm) for the selected carbons of compounds **9f-9h** 156

Table 4.20 The phase transition temperatures (°C), associated enthalpy changes (kJmol^{-1}) and nematic-isotropic entropy changes of compounds **9a-9h** (● = enantiotropic phase, Cr = crystal, N = nematic, I = isotropic) 158

Table 5.1 C and H microanalytical data of compound **10** 165

Table 5.2 Selected FT-IR absorption frequency (υ / cm^{-1}) of compound **10** 166

Table 5.3 List of ^{1}H-NMR chemical shifts (δ / ppm), multiplicity, number of protons and associated functional groups of compound **10** 166

Table 5.4 C, H and N microanalytical data of compound **11** 170

Table 5.5 Selected FT-IR absorption frequency (υ / cm^{-1}) of compound **11** 170

Table 5.6 Yields (%) of compounds **12a-12h** 173

Table 5.7 C, H and N microanalytical data of compounds **12a-12h** 173

Table 5.8 Selected FT-IR absorption frequency (υ / cm^{-1}) of compounds **12a-12h** 174

Table 5.9 List of ^{1}H-NMR chemical shifts (δ / ppm), multiplicity, number of protons and associated functional groups of compounds **12a-12h** 180

Table 5.10 Yields (%) of compounds **13a-13h** 181

Table 5.11 C, H and N microanalytical data of compounds **13a-13h** 182

Table 5.12 Selected FT-IR absorption frequency (υ / cm^{-1}) of compounds **13a-13h** 185

Table 5.13 Chemical shifts (δ / ppm) for the selected protons of compound **13c** 187

Table 5.14 Chemical shifts (δ / ppm) for the selected carbons and ^{1}H-^{13}C HMQC and HMBC correlations of compound **13c** 191

Table 5.15 Chemical shifts (δ / ppm) for the quaternary carbons of compound **13c** 198

Table 5.16 Chemical shifts (δ / ppm) for the selected protons of compound **13f** 202

Table 5.17 Chemical shifts (δ / ppm) for the selected carbons and ^{1}H-^{13}C HMQC and HMBC correlations of compound **13f** 210

Table 5.18 Chemical shifts (δ / ppm) for the quaternary carbons of compound **13f** 211

Table 5.19 Chemical shifts (δ / ppm) for the selected protons of compounds **13a**, **13b**, **13d**, **13e**, **13g** and **13h** 211

Table 5.20 Chemical shifts (δ / ppm) for the selected carbons of compounds **13a**, **13b**, **13d**, **13e**, **13g** and **13h** 212

Table 5.21 The phase transition temperatures (°C) and associated enthalpy changes (kJmol^{-1}) of compounds **13a-13h**. Only the highest melting points are listed. (● = enantiotropic phase, ○ = monotropic phase, Cr = crystal, SmX = unidentified smectic, SmC* = chiral smectic C, SmA = smectic A, N* = chiral nematic, BP = blue phase, I = isotropic) 214

Table 6.1 C, H and N microanalytical data of compound **14** 227

Table 6.2 Selected FT-IR absorption frequency (υ / cm^{-1}) of compound **14** 227

Table 6.3 Yields (%) of compounds **15a-15h** 230

Table 6.4 C, H and N microanalytical data of compounds **15a-15h** 230

Table 6.5 Selected FT-IR absorption frequency (υ / cm^{-1}) of compounds **15a-15h** 231

Table 6.6 List of ^{1}H-NMR chemical shifts (δ / ppm), multiplicity, number of protons and associated functional groups of compounds **15a-15h** 237

Table 6.7 Yields (%) of compounds **16a-16h** 239

Table 6.8 C, H and N microanalytical data of compounds **16a-16h** 239

Table 6.9 Selected FT-IR absorption frequency (υ / cm^{-1}) of compounds **16a-16h** 240

Table 6.10 Chemical shifts (δ / ppm) for the selected protons of compound **16e** 245

Table 6.11 Chemical shifts (δ / ppm) for the selected carbons and ^{1}H-^{13}C HMQC and HMBC correlations of compound **16e** 249

Table 6.12 Chemical shifts (δ / ppm) for the quaternary carbons of compound **16e** 256

Table 6.13 Chemical shifts (δ / ppm) for the selected protons of compound **16f** 257

Table 6.14 Chemical shifts (δ / ppm) for the selected carbons and ^{1}H-^{13}C HMQC and HMBC correlations of compound **16f** 265

Table 6.15 Chemical shifts (δ / ppm) for the quaternary carbons of compound **16f** 268

Table 6.16 Chemical shifts (δ / ppm) for the selected protons of compounds **16a-16d**, **16g** and **16h** 269

Table 6.17 Chemical shifts (δ / ppm) for the selected carbons of compounds **16a-16d**, **16g** and **16h** 269

Table 6.18 Phase transition temperatures (°C) and associated enthalpy changes (kJmol^{-1}) of compounds **16a-16h**. Only the highest melting points are listed. (● = enantiotropic phase, Cr = crystal, N* = chiral nematic, I = isotropic) 271

Table 7.1 C, H and N microanalytical data of compound **17** 275

Table 7.2 Selected FT-IR absorption frequency (υ / cm^{-1}) of compound **17** 275

Table 7.3 Yields (%) of compounds **18a-18h** 278

Table 7.4 C, H and N microanalytical data of compounds **18a-18h** 278

Table 7.5 Selected FT-IR absorption frequency (υ / cm^{-1}) of compounds **18a-18h** 281

Table 7.6 List of ^{1}H-NMR chemical shifts (δ / ppm), multiplicity, number of protons and associated functional groups of compounds **18a-18h** 282

Table 7.7 Yields (%) of compounds **19a-19h** 286

Table 7.8 C, H and N microanalytical data of compounds **19a-19h** 286

Table 7.9 Selected FT-IR absorption frequency (υ / cm^{-1}) of compounds **19a-19h** 287

Table 7.10 Chemical shifts (δ / ppm) for the selected protons of compound **19d** 292

Table 7.11 Chemical shifts (δ / ppm) for the selected carbons and ^{1}H-^{13}C HMQC and HMBC correlations of compound **19d** 300

Table 7.12 Chemical shifts (δ / ppm) for the quaternary carbons of compound **19d** 303

Table 7.13 Chemical shifts (δ / ppm) for the selected protons of compound **19e** 307

Table 7.14 Chemical shifts (δ / ppm) for the selected carbons and ^{1}H-^{13}C HMQC and HMBC correlations of compound **19e** 309

Table 7.15 Chemical shifts (δ / ppm) for the quaternary carbons of compound **19e** 315

Table 7.16 Chemical shifts (δ / ppm) for the selected protons of compounds **19a-19c** and **19f-19h** 316

Table 7.17 Chemical shifts (δ / ppm) for the selected carbons of compounds **19a-19c** and **19f-19h** 316

Table 7.18 Phase transition temperatures (°C), associated enthalpy changes ($kJmol^{-1}$) and chiral nematic-isotropic entropy changes of compounds **19a-19h**. Only the highest melting points are listed. (● = enantiotropic phase, ○ = monotropic phase, Cr = crystal, N* = chiral nematic, BP = blue phase, I = isotropic) 317

Table 8.1 C, H and N microanalytical data of compounds **23a-23d** 329

Table 8.2 Selected FT-IR absorption frequency (υ / cm^{-1}) of compounds **23a-23d** 329

Table 8.3 List of ^{1}H-NMR chemical shifts (δ / ppm), multiplicity, number of protons and associated functional groups of compounds **23a-23d** 332

Table 8.4 C, H and N microanalytical data of compounds **24a-24d** 336

Table 8.5 Selected FT-IR absorption frequency (υ / cm^{-1}) of compounds **24a-24d** 339

Table 8.6 List of ^{1}H-NMR chemical shifts (δ / ppm), multiplicity, number of protons and associated functional groups of compounds **24a-24d** 342

Table 8.7 Yields (%) of compounds **25a-25d** and **26a-26d** 344

Table 8.8 C, H and N microanalytical data of compounds **25a-25d** and **26a-26d** 344

Table 8.9 Selected FT-IR absorption frequency (υ / cm^{-1}) of compounds **25a-25d** and **26a-26d** 345

Table 8.10 Chemical shifts (δ / ppm) for the selected protons of compound **25a** 353

Table 8.11 Chemical shifts (δ / ppm) for the selected carbons and ^{1}H-^{13}C HMQC and HMBC correlations of compound **25a** 355

Table 8.12 Chemical shifts (δ / ppm) for the quaternary carbons of compound **25a** 362

Table 8.13 Chemical shifts (δ / ppm) for the selected protons of compound **26c** 366

Table 8.14 Chemical shifts (δ / ppm) for the selected carbons and ^{1}H-^{13}C HMQC and HMBC correlations of compound **26c** 374

Table 8.15 Chemical shifts (δ / ppm) for the quaternary carbons of compound **26c** 375

Table 8.16 Chemical shifts (δ / ppm) for the selected protons of compounds **25b**, **25c**, **25d**, **26a**, **26b** and **26d** 376

Table 8.17 Chemical shifts (δ / ppm) for the selected carbons of compounds **25b**, **25c**, and **25d** 377

Table 8.18 Chemical shifts (δ / ppm) for the selected carbons of compounds **26a**, **26b**, and **26d** 378

Table 8.19 Phase transition temperatures (°C) and associated enthalpy changes ($kJmol^{-1}$) of compounds **24a-24d**, **25a-25d** and **26a-26d**. Only the highest melting points are listed. (● = enantiotropic phase, ○ = monotropic phase, T_g = glass transition temperature, Cr = crystal, N = nematic, I = isotropic) 380

LIST OF FIGURES

Figure 1.1 Primary phase transitions and phase transitions involving liquid crystalline phase (in dotted box) 2

Figure 1.2 Nematic phase (Barón, 2001) 3

Figure 1.3 Chiral nematic phase (Barón, 2001) 4

Figure 1.4 Molecular arrangement in (a) SmA phase with *Z* = optic axis; (b) SmC phase (Barón, 2001) 6

Figure 1.5 SmB phase (Barón, 2001) 7

Figure 1.6 Illustration of the respective tilt directions of the director in the (a) SmF; (b) SmI phases 7

Figure 1.7 SmC* phase with *P* = helical pitch (Barón, 2001) 8

Figure 1.8 A blue phase model consisting of double-twist cylinders forming a cubic lattice (Barón, 2001) 10

Figure 1.9 Two examples of calamitic mesogens (a) N-[4-(4-octyloxybenzoyloxy)-2-hydroxybenzylidene]-3-aminopyridine (Takase *et al*., 2003); (b) 4-[(S)-2-chloro-4-methylpentanoyloxy]-4’-[4-propylbenzoyloxy]-biphenyl (Schacht *et al*., 1998) 11

Figure 1.10 Inositol ether (Tschierske, 1998) 11

Figure 1.11 4,6-Dichloro-1,3-phenylenebis[4-(4-*n*-octyloxyphenyliminomethyl)-benzoate] (Lee *et al*., 2003) 12

Figure 1.12 4-Dodecyloxy-2’-(4-butoxybenzoyloxy)-4’-(4-butoxybenzoyloxy)-azobenzenes (Berdagué *et al*., 1993) 13

Figure 1.13 Respective example of symmetric dimer and non-symmetric dimer (a) α,ω-bis(4-pentylanilinebenzylidene-4’-oxy)butane (Date *et al*., 1992); (b) α-(4-cyanobiphenyl-4’-oxy)-ω-(4-butylaniline-benzylidene-4’-oxy)hexane (Hogan *et al*., 1988) 14

Figure 1.14 Structure for the dimer which contains cholesterol and 4-(*trans*-4-*n*-hexylcyclohexyl)benzoic acid moieties (Yu *et al*., 2008) 14

Figure 1.15 Respective example of symmetric trimer and non-symmetric trimer (a) 4,4’-bis[ω-(4-cyanobiphenyl-4’-yloxy)butyloxy]biphenyl; (b) mesogen incorporating 5-octylpyrimidine-2-yl and 4-cyanophenyl moieties (Yoshizawa *et al*., 2005) 15

Figure 2.1 Overall synthetic routes towards obtaining compounds **4a-4j** 26

Figure 2.2 Overall synthetic routes towards obtaining compounds **9a-9h** 29

Figure 2.3 Overall synthetic routes towards obtaining compounds **13a-13h**, **16a-16h** and **19a-19h** 33

Figure 2.4 Overall synthetic routes towards obtaining compounds **25a-25d** and **26a-26d** 38

Figure 3.1 Esterification reaction between 4-(4-hydroxyphenyl)benzoic acid and (*RS*)-2-methyl-1-butanol to yield (*RS*)-2-methylbutyl-4’-(4”-hydroxyphenyl)benzoate, **1** 42

Figure 3.2 Mechanism for the Fischer acid-catalyzed esterification reaction between 4-(4-hydroxyphenyl)benzoic acid and (*RS*)-2-methyl-1-butanol to yield compound **1** 43

Figure 3.3 FT-IR spectrum of (*RS*)-2-methylbutyl-4’-(4”-hydroxyphenyl)-benzoate, **1** 45

Figure 3.4 Resonance structure for (*RS*)-2-methylbutyl-4’-(4”-hydroxyphenyl)-benzoate, **1** 46

Figure 3.5 Atom numbering for the branched alkyl fragment of compound **1** 46

Figure 3.6 ^{1}H-NMR spectrum of (*RS*)-2-methylbutyl-4’-(4”-hydroxyphenyl)-benzoate, **1** 49

Figure 3.7 Condensation reaction between 4-hydroxybenzaldehyde and various 4-substituted-anilines to yield 4-hydroxy-4’-benzylidene-substituted-anilines, **2a-2e** 50

Figure 3.8 Mechanism for the condensation reaction between 4-hydroxybenzaldehyde and 4-methylaniline to yield compound **2b** 51

Figure 3.9 FT-IR spectrum of 4-hydroxy-4’-benzylidenemethylaniline, **2b** and examples of band assignment to the different functional groups 54

Figure 3.10 FT-IR spectrum of 4-hydroxy-4’-benzylidenechloroaniline, **2d** 55

Figure 3.11 Atom numbering for the aromatic protons of compound **2** 57

Figure 3.12 ^{1}H-NMR spectrum of 4-hydroxy-4’-benzylidenemethylaniline, **2b** and examples of peak assignment to the different types of proton 58

Figure 3.13 ^{1}H-NMR spectrum of 4-hydroxy-4’-benzylidenechloroaniline, **2d** 59

Figure 3.14 Etherification reaction between compounds **2a-2e** and 1,6-dibromohexane and 1,8-dibromooctane to yield 4-(*n*-bromoalkyloxy)-4’-benzylidene-substituted-anilines, **3a-3j** 61

Figure 3.15 Mechanism for the Williamson ether synthetic reaction between the phenoxide ion of compound **2b** and 1,6-dibromohexane to yield compound **3b** 61

Figure 3.16 FT-IR spectrum of 4-(6-bromohexyloxy)-4’-benzylidenemethylaniline, **3b** and examples of band assignment to the different functional groups 64

Figure 3.17 FT-IR spectrum of 4-(6-bromohexyloxy)-4’-benzylidenechloroaniline, **3d** 65

Figure 3.18 Atom numbering for the aromatic protons of compound **3** 67

Figure 3.19 ^{1}H-NMR spectrum of 4-(6-bromohexyloxy)-4’-benzylidenemethylaniline, **3b** and examples of peak assignment to the different types of proton 69

Figure 3.20 ^{1}H-NMR spectrum of 4-(6-bromohexyloxy)-4’-benzylidenechloroaniline, **3d** 70

Figure 3.21 Etherification reaction between compound **1** and compounds **3a**-**3j** to yield α-(4-benzylidene-substituted-aniline-4’-oxy)-ω-[2-methylbutyl-4’-(4”-phenyl)benzoateoxy]alkanes, **4a**-**4j** 72

Figure 3.22 FT-IR spectrum of α-(4-benzylidenemethylaniline-4’-oxy)-ω-[2-methylbutyl-4’-(4”-phenyl)benzoateoxy]hexane, **4b** and examples of band assignment to the different functional groups 76

Figure 3.23 FT-IR spectrum of α-(4-benzylidenechloroaniline-4’-oxy)-ω-[2-methylbutyl-4’-(4”-phenyl)benzoateoxy]hexane, **4d** 77

Figure 3.24 Atom numbering for compound **4b** 78

Figure 3.25 ^{1}H-NMR spectrum of α-(4-benzylidenemethylaniline-4’-oxy)-ω-[2-methylbutyl-4’-(4”-phenyl)benzoateoxy]hexane, **4b** and examples of peak assignment to the different types of proton 79

Figure 3.26 (a) ^{1}H-^{1}H COSY spectrum of α-(4-benzylidenemethylaniline-4’-oxy)-ω-[2-methylbutyl-4’-(4”-phenyl)benzoateoxy]hexane, **4b**; (b) representations of some deduced ^{1}H-^{1}H COSY correlations 82

Figure 3.27 ^{13}C-NMR spectrum of α-(4-benzylidenemethylaniline-4’-oxy)-ω-[2-methylbutyl-4’-(4”-phenyl)benzoateoxy]hexane, **4b** 84

Figure 3.28 DEPT 90 spectrum of α-(4-benzylidenemethylaniline-4’-oxy)-ω-[2-methylbutyl-4’-(4”-phenyl)benzoateoxy]hexane, **4b** 85

Figure 3.29 DEPT 135 spectrum of α-(4-benzylidenemethylaniline-4’-oxy)-ω-[2-methylbutyl-4’-(4”-phenyl)benzoateoxy]hexane, **4b** 86

Figure 3.30 (a) ^{1}H-^{13}C HMQC spectrum of α-(4-benzylidenemethylaniline-4'-oxy)-ω-[2-methylbutyl-4'-(4"-phenyl)benzoateoxy]hexane, **4b**; (b) representations of some deduced ^{1}H-^{13}C HMQC correlations 87

Figure 3.31 (a) ^{1}H-^{13}C HMBC spectrum of α-(4-benzylidenemethylaniline-4'-oxy)-ω-[2-methylbutyl-4'-(4"-phenyl)benzoateoxy]hexane, **4b**; (b) representations of some deduced ^{1}H-^{13}C HMBC correlations 89

Figure 3.32 Atom numbering for compound **4d** 93

Figure 3.33 ^{1}H-NMR spectrum of α-(4-benzylidenechloroaniline-4'-oxy)-ω-[2-methylbutyl-4'-(4"-phenyl)benzoateoxy]hexane, **4d** 94

Figure 3.34 (a) ^{1}H-^{1}H COSY spectrum of α-(4-benzylidenechloroaniline-4'-oxy)-ω-[2-methylbutyl-4'-(4"-phenyl)benzoateoxy]hexane, **4d**; (b) representations of some deduced ^{1}H-^{1}H COSY correlations 95

Figure 3.35 ^{13}C-NMR spectrum of α-(4-benzylidenechloroaniline-4'-oxy)-ω-[2-methylbutyl-4'-(4"-phenyl)benzoateoxy]hexane, **4d** 98

Figure 3.36 DEPT 90 spectrum of α-(4-benzylidenechloroaniline-4'-oxy)-ω-[2-methylbutyl-4'-(4"-phenyl)benzoateoxy]hexane, **4d** 99

Figure 3.37 DEPT 135 spectrum of α-(4-benzylidenechloroaniline-4'-oxy)-ω-[2-methylbutyl-4'-(4"-phenyl)benzoateoxy]hexane, **4d** 100

Figure 3.38 (a) ^{1}H-^{13}C HMQC spectrum of α-(4-benzylidenechloroaniline-4'-oxy)-ω-[2-methylbutyl-4'-(4"-phenyl)benzoateoxy]hexane, **4d**; (b) representations of some deduced ^{1}H-^{13}C HMQC correlations 101

Figure 3.39 (a) ^{1}H-^{13}C HMBC spectrum of α-(4-benzylidenechloroaniline-4'-oxy)-ω-[2-methylbutyl-4'-(4"-phenyl)benzoateoxy]hexane, **4d**; (b) representations of some deduced ^{1}H-^{13}C HMBC correlations 102

Figure 3.40 DSC trace of compound **4c** on heating and cooling cycles at the rate of ±2 ^{o}Cmin^{-1} 110

Figure 3.41 Schlieren texture of the nematic phase of compound **4i** at 131.4 °C 111

Figure 3.42 Focal conic fan texture containing polygonal defects of the SmA phase of compound **4e** at 114.5 ^{o}C 111

Figure 3.43 Derived intensity versus 2θ profile of the X-ray diffraction powder pattern of compound **4e** in the intercalated SmA phase at 110 ^{o}C. The inset shows the intensity versus 2θ profile in the Cr phase at 100 ^{o}C. 113

Figure 3.44 Sketch of the molecular organization within the intercalated SmA phase shown by **4e**. The layer periodicity is indicated as 18.3 Å. 114

Figure 4.1 Esterification reaction between 4-hydroxybenzaldehyde and 2-thiophenecarbonyl chloride to yield 4-formylphenyl thiophene-2-carboxylate, **5** 118

Figure 4.2 Mechanism for the Schotten-Baumann esterification reaction between 4-hydroxybenzaldehyde and 2-thiophenecarbonyl chloride to yield compound **5** 119

Figure 4.3 FT-IR spectrum of 4-formylphenyl thiophene-2-carboxylate, **5** 122

Figure 4.4 ^{1}H-NMR spectrum of 4-formylphenyl thiophene-2-carboxylate, **5** 123

Figure 4.5 Condensation reaction between 4-aminophenol and compound **5** to yield 4-(thiophene-2-carboxyl)benzylidene-4'-hydroxyaniline, **6** 124

Figure 4.6 FT-IR spectrum of 4-(thiophene-2-carboxyl)benzylidene-4'-hydroxyaniline, **6** 128

Figure 4.7 ^{1}H-NMR spectrum of 4-(thiophene-2-carboxyl)benzylidene-4'-hydroxyaniline, **6** 129

Figure 4.8 Etherification reaction between compound **7** and a series of α,ω-dibromoalkanes to yield 4-(*n*-bromoalkyloxy)-4'-benzylidene-chloroanilines, **8a-8h** 130

Figure 4.9 FT-IR spectrum of 4-(7-bromoheptyloxy)-4'-benzylidenechloro-aniline, **8c** 132

Figure 4.10 ^{1}H-NMR spectrum of 4-(7-bromoheptyloxy)-4'-benzylidenechloro-aniline, **8c** 134

Figure 4.11 Etherification reaction between compound **6** and compounds **8a-8h** to yield α-(4-benzylidenechloroaniline-4'-oxy)-ω-[4-(thiophene-2-carboxyl)benzylideneaniline-4'-oxy]alkanes, **9a-9h** 136

Figure 4.12 FT-IR spectrum of α-(4-benzylidenechloroaniline-4'-oxy)-ω-[4-(thiophene-2-carboxyl)benzylideneaniline-4'-oxy]heptane, **9c** 139

Figure 4.13 Atom numbering for compound **9c** 140

Figure 4.14 ^{1}H-NMR spectrum of α-(4-benzylidenechloroaniline-4'-oxy)-ω-[4-(thiophene-2-carboxyl)benzylideneaniline-4'-oxy]heptane, **9c** 143

Figure 4.15 (a) ^{1}H-^{1}H COSY spectrum of α-(4-benzylidenechloroaniline-4'-oxy)-ω-[4-(thiophene-2-carboxyl)benzylideneaniline-4'-oxy]heptane, **9c**; (b) representations of some deduced ^{1}H-^{1}H COSY correlations 144

Figure 4.16 ^{13}C-NMR spectrum of α-(4-benzylidenechloroaniline-4'-oxy)-ω-[4-(thiophene-2-carboxyl)benzylideneaniline-4'-oxy]heptane, **9c** 146

Figure 4.17 DEPT 90 spectrum of α-(4-benzylidenechloroaniline-4’-oxy)-ω-[4-(thiophene-2-carboxyl)benzylideneaniline-4’-oxy]heptane, **9c** 147

Figure 4.18 DEPT 135 spectrum of α-(4-benzylidenechloroaniline-4’-oxy)-ω-[4-(thiophene-2-carboxyl)benzylideneaniline-4’-oxy]heptane, **9c** 148

Figure 4.19 (a) ^{1}H-^{13}C HMQC spectrum of α-(4-benzylidenechloroaniline-4’-oxy)-ω-[4-(thiophene-2-carboxyl)benzylideneaniline-4’-oxy]heptane, **9c**; (b) representations of some deduced ^{1}H-^{13}C HMQC correlations 152

Figure 4.20 (a) ^{1}H-^{13}C HMBC spectrum of α-(4-benzylidenechloroaniline-4’-oxy)-ω-[4-(thiophene-2-carboxyl)benzylideneaniline-4’-oxy]heptane, **9c**; (b) representations of some deduced ^{1}H-^{13}C HMBC correlations 153

Figure 4.21 Dependence of phase transition temperatures, T on the number of methylene units, *n* in the flexible spacer 159

Figure 4.22 Comparison of N phase temperature range, T between odd and even members during heating run 159

Figure 4.23 DSC trace of compound **9d** with heating and cooling rates of ±5 °Cmin^{-1} 160

Figure 4.24 Dependence of the entropy change ($\Delta S_{NI}/R$) associated with the nematic-isotropic transition on the number of methylene units, *n* in the flexible spacer 161

Figure 4.25 N schlieren texture (compound **9g**) with both twofold and fourfold brushes at 186.0 °C 162

Figure 4.26 Filaments observed in the homeotropic region of N phase (compound **9f**) which initially form (left) upon cooling and gradually transform to compact domain (right) 163

Figure 5.1 Esterification reaction between 4-(4-hydroxyphenyl)benzoic acid and (*S*)-(-)-2-methyl-1-butanol to yield (*S*)-(-)-2-methylbutyl-4’-(4”-hydroxylphenyl)benzoate, **10** 164

Figure 5.2 FT-IR spectrum of (*S*)-(-)-2-methylbutyl-4’-(4”-hydroxyphenyl)-benzoate, **10** 167

Figure 5.3 ^{1}H-NMR spectrum of (*S*)-(-)-2-methylbutyl-4’-(4”-hydroxy-phenyl)benzoate, **10** 168

Figure 5.4 Condensation reaction between 1,4-diaminobenzene and 4-hydroxybenzaldehyde to yield 4,4’-bis(4-hydroxybenzylidene)-1,4-diaminobenzene, **11** 169

Figure 5.5 FT-IR spectrum of 4,4’-bis(4-hydroxybenzylidene)-1,4-diaminobenzene, **11** 171

Figure 5.6 Etherification reaction between compound **11** and a series of α,ω-dibromoalkanes to yield 4,4’-bis[4-(*n*-bromoalkyloxy)benzylidene]-1,4-diaminobenzenes, **12a**-**12h** 172

Figure 5.7 FT-IR spectrum of 4,4’-bis[4-(7-bromoheptyloxy)benzylidene]-1,4-diaminobenzene, **12c** 175

Figure 5.8 FT-IR spectrum of 4,4’-bis[4-(10-bromodecyloxy)benzylidene]-1,4-diaminobenzene, **12f** 176

Figure 5.9 ^{1}H-NMR spectrum of 4,4’-bis[4-(7-bromoheptyloxy)benzylidene]-1,4-diaminobenzene, **12c** 178

Figure 5.10 ^{1}H-NMR spectrum of 4,4’-bis[4-(10-bromodecyloxy)benzylidene]-1,4-diaminobenzene, **12f** 179

Figure 5.11 Etherification reaction between compound **10** and compounds **12a**-**12h** to yield 4,4’-bis{ω-[2-methylbutyl-4’-(4”-phenyl)benzoateoxy]-alkyloxybenzylidene}-1,4-diaminobenzenes, **13a**-**13h** 181

Figure 5.12 FT-IR spectrum of 4,4’-bis{ω-[2-methylbutyl-4’-(4”-phenyl)-benzoateoxy]heptyloxybenzylidene}-1,4-diaminobenzene, **13c** 183

Figure 5.13 FT-IR spectrum of 4,4’-bis{ω-[2-methylbutyl-4’-(4”-phenyl)-benzoateoxy]decyloxybenzylidene}-1,4-diaminobenzene, **13f** 184

Figure 5.14 Atom numbering for compound **13c** 185

Figure 5.15 ^{1}H-NMR spectrum of 4,4’-bis{ω-[2-methylbutyl-4’-(4”-phenyl)-benzoateoxy]heptyloxybenzylidene}-1,4-diaminobenzene, **13c** 188

Figure 5.16 (a) ^{1}H-^{1}H COSY spectrum of 4,4’-bis{ω-[2-methylbutyl-4’-(4”-phenyl)benzoateoxy]heptyloxybenzylidene}-1,4-diaminobenzene, **13c**; (b) representations of some deduced ^{1}H-^{1}H COSY correlations 189

Figure 5.17 ^{13}C-NMR spectrum of 4,4’-bis{ω-[2-methylbutyl-4’-(4”-phenyl)-benzoateoxy]heptyloxybenzylidene}-1,4-diaminobenzene, **13c** 192

Figure 5.18 DEPT 90 spectrum of 4,4’-bis{ω-[2-methylbutyl-4’-(4”-phenyl)-benzoateoxy]heptyloxybenzylidene}-1,4-diaminobenzene, **13c** 193

Figure 5.19 DEPT 135 spectrum of 4,4’-bis{ω-[2-methylbutyl-4’-(4”-phenyl)-benzoateoxy]heptyloxybenzylidene}-1,4-diaminobenzene, **13c** 194

Figure 5.20 (a) ^{1}H-^{13}C HMQC spectrum of 4,4’-bis{ω-[2-methylbutyl-4’-(4”-phenyl)benzoateoxy]heptyloxybenzylidene}-1,4-diaminobenzene, **13c**; (b) representations of some deduced ^{1}H-^{13}C HMQC correlations 195

Figure 5.21 (a) ^{1}H-^{13}C HMBC spectrum of 4,4’-bis{ω-[2-methylbutyl-4’-(4”-phenyl)benzoateoxy]heptyloxybenzylidene}-1,4-diaminobenzene, **13c**; (b) representations of some deduced ^{1}H-^{13}C HMBC correlations 197

Figure 5.22 Atom numbering for compound **13f** 198

Figure 5.23 ^{1}H-NMR spectrum of 4,4’-bis{ω-[2-methylbutyl-4’-(4”-phenyl)-benzoateoxy]decyloxybenzylidene}-1,4-diaminobenzene, **13f** 200

Figure 5.24 (a) ^{1}H-^{1}H COSY spectrum of 4,4’-bis{ω-[2-methylbutyl-4’-(4”-phenyl)benzoateoxy]decyloxybenzylidene}-1,4-diaminobenzene, **13f**; (b) representations of some deduced ^{1}H-^{1}H COSY correlations 201

Figure 5.25 ^{13}C-NMR spectrum of 4,4’-bis{ω-[2-methylbutyl-4’-(4”-phenyl)-benzoateoxy]decyloxybenzylidene}-1,4-diaminobenzene, **13f** 205

Figure 5.26 DEPT 90 spectrum of 4,4’-bis{ω-[2-methylbutyl-4’-(4”-phenyl)-benzoateoxy]decyloxybenzylidene}-1,4-diaminobenzene, **13f** 206

Figure 5.27 DEPT 135 spectrum of 4,4’-bis{ω-[2-methylbutyl-4’-(4”-phenyl)-benzoateoxy]decyloxybenzylidene}-1,4-diaminobenzene, **13f** 207

Figure 5.28 (a) ^{1}H-^{13}C HMQC spectrum of 4,4’-bis{ω-[2-methylbutyl-4’-(4”-phenyl)benzoateoxy]decyloxybenzylidene}-1,4-diaminobenzene, **13f**; (b) representations of some deduced ^{1}H-^{13}C HMQC correlations 208

Figure 5.29 (a) ^{1}H-^{13}C HMBC spectrum of 4,4’-bis{ω-[2-methylbutyl-4’-(4”-phenyl)benzoateoxy]decyloxybenzylidene}-1,4-diaminobenzene, **13f**; (b) representations of some deduced ^{1}H-^{13}C HMBC correlations 209

Figure 5.30 Dependence of the transition temperatures on the number of methylene units, *n* in the flexible spacers for compounds **13a**-**13h** 215

Figure 5.31 DSC trace of compound **13a** with heating and cooling rate of ±5 °Cmin^{-1} 215

Figure 5.32 SmA fan-shaped texture of compound **13d** at 198.2 °C upon heating 217

Figure 5.33 Dependence of smectic layer spacing on temperature for
(a) compound **13a** 217
(b) compound **13c** 218
(c) compound **13e** 218
(d) compound **13f** and 219
(e) compound **13g** 219

Figure 5.34 Photomicrograph of the monotropic SmF* mosaic-schlieren texture of compound **13c** upon cooling the SmC* phase 222

Figure 5.35 Evolution from
(a) the SmA homeotropic texture at 164.4 °C to 222
(b) pseudo-homeotropic texture of the SmC* phase at 152.0 °C to 222
(c) the coexistence of homeotropic and platelet / fan-like texture of the SmX phase at 136.0 °C 222

Figure 5.36 Mosaic texture of the monotropic SmX phase of compound **13e** 223

Figure 5.37 Proposed conformation of **13f** based on MM2 minimum energetic parameters 223

Figure 5.38 Proposed SmA_1 molecular organization model for compound **13f** with layer spacing of 72.6 Å 224

Figure 5.39 Platelet texture of the blue phase (compound **13e**) upon cooling the isotropic phase 225

Figure 6.1 Condensation reaction between 1,4-diaminobenzene and vanillin to yield 4,4’-bis(3-methoxy-4-hydroxybenzylidene)-1,4-diaminobenzene, **14** 226

Figure 6.2 FT-IR spectrum of 4,4’-bis(3-methoxy-4-hydroxybenzylidene)-1,4-diaminobenzene, **14** 228

Figure 6.3 Etherification reaction between compound **14** and a series of α,ω-dibromoalkanes to yield 4,4’-bis[3-methoxy-4-(*n*-bromoalkyloxy)-benzylidene]-1,4-diaminobenzenes, **15a-15h** 229

Figure 6.4 FT-IR spectrum of 4,4’-bis[3-methoxy-4-(9-bromononyloxy)-benzylidene]-1,4-diaminobenzene, **15e** 232

Figure 6.5 FT-IR spectrum of 4,4’-bis[3-methoxy-4-(10-bromodecyloxy)-benzylidene]-1,4-diaminobenzene, **15f** 233

Figure 6.6 ^{1}H-NMR spectrum of 4,4’-bis[3-methoxy-4-(9-bromononyloxy)-benzylidene]-1,4-diaminobenzene, **15e** 235

Figure 6.7 ^{1}H-NMR spectrum of 4,4’-bis[3-methoxy-4-(10-bromodecyloxy)-benzylidene]-1,4-diaminobenzene, **15f** 236

Figure 6.8 Etherification reaction between compound **10** and compounds **15a-15h** to yield 4,4’-bis{ω-[2-methylbutyl-4’-(4”-phenyl)-benzoateoxy]-3-methoxy-4-alkyloxybenzylidene}-1,4-diaminobenzenes, **16a-16h** 238

Figure 6.9 FT-IR spectrum of 4,4’-bis{ω-[2-methylbutyl-4’-(4”-phenyl)-benzoateoxy]-3-methoxy-4-nonyloxybenzylidene}-1,4-diaminobenzene, **16e** 241

Figure 6.10 FT-IR spectrum of 4,4’-bis{ω-[2-methylbutyl-4’-(4”-phenyl)-benzoateoxy]-3-methoxy-4-decyloxybenzylidene}-1,4-diaminobenzene, **16f** 242

Figure 6.11 Atom numbering for compound **16e** 243

Figure 6.12 ^{1}H-NMR spectrum of 4,4’-bis{ω-[2-methylbutyl-4’-(4”-phenyl)-benzoateoxy]-3-methoxy-4-nonyloxybenzylidene}-1,4-diaminobenzene, **16e** 246

Figure 6.13 (a) ^{1}H-^{1}H COSY spectrum of 4,4’-bis{ω-[2-methylbutyl-4’-(4”-phenyl)benzoateoxy]-3-methoxy-4-nonyloxybenzylidene}-1,4-diaminobenzene, **16e**; (b) representations of some deduced ^{1}H-^{1}H COSY correlations 247

Figure 6.14 ^{13}C-NMR spectrum of 4,4’-bis{ω-[2-methylbutyl-4’-(4”-phenyl)-benzoateoxy]-3-methoxy-4-nonyloxybenzylidene}-1,4-diaminobenzene, **16e** 250

Figure 6.15 DEPT 90 spectrum of 4,4’-bis{ω-[2-methylbutyl-4’-(4”-phenyl)-benzoateoxy]-3-methoxy-4-nonyloxybenzylidene}-1,4-diaminobenzene, **16e** 251

Figure 6.16 DEPT 135 spectrum of 4,4’-bis{ω-[2-methylbutyl-4’-(4”-phenyl)-benzoateoxy]-3-methoxy-4-nonyloxybenzylidene}-1,4-diaminobenzene, **16e** 252

Figure 6.17 (a) ^{1}H-^{13}C HMQC spectrum of 4,4’-bis{ω-[2-methylbutyl-4’-(4”-phenyl)benzoateoxy]-3-methoxy-4-nonyloxybenzylidene}-1,4-diaminobenzene, **16e**; (b) representations of some deduced ^{1}H-^{13}C HMQC correlations 253

Figure 6.18 (a) ^{1}H-^{13}C HMBC spectrum of 4,4’-bis{ω-[2-methylbutyl-4’-(4”-phenyl)benzoateoxy]-3-methoxy-4-nonyloxybenzylidene}-1,4-diaminobenzene, **16e**; (b) representations of some deduced ^{1}H-^{13}C HMBC correlations 255

Figure 6.19 Atom numbering for compound **16f** 256

Figure 6.20 ^{1}H-NMR spectrum of 4,4’-bis{ω-[2-methylbutyl-4’-(4”-phenyl)-benzoateoxy]-3-methoxy-4-decyloxybenzylidene}-1,4-diaminobenzene, **16f** 258

Figure 6.21 (a) ^{1}H-^{1}H COSY spectrum of 4,4’-bis{ω-[2-methylbutyl-4’-(4”-phenyl)benzoateoxy]-3-methoxy-4-decyloxybenzylidene}-1,4-diaminobenzene, **16f**; (b) representations of some deduced ^{1}H-^{1}H COSY correlations 259

Figure 6.22 ^{13}C-NMR spectrum of 4,4’-bis{ω-[2-methylbutyl-4’-(4”-phenyl)benzoateoxy]-3-methoxy-4-decyloxybenzylidene}-1,4-diaminobenzene, **16f** 261

Figure 6.23 DEPT 90 spectrum of 4,4’-bis{ω-[2-methylbutyl-4’-(4”-phenyl)benzoateoxy]-3-methoxy-4-decyloxybenzylidene}-1,4-diaminobenzene, **16f** 262

Figure 6.24 DEPT 135 spectrum of 4,4’-bis{ω-[2-methylbutyl-4’-(4”-phenyl)benzoateoxy]-3-methoxy-4-decyloxybenzylidene}-1,4-diaminobenzene, **16f** 263

Figure 6.25 (a) ^{1}H-^{13}C HMQC spectrum of 4,4’-bis{ω-[2-methylbutyl-4’-(4”-phenyl)benzoateoxy]-3-methoxy-4-decyloxybenzylidene}-1,4-diaminobenzene, **16f**; (b) representations of some deduced ^{1}H-^{13}C HMQC correlations 264

Figure 6.26 (a) ^{1}H-^{13}C HMBC spectrum of 4,4’-bis{ω-[2-methylbutyl-4’-(4”-phenyl)benzoateoxy]-3-methoxy-4-decyloxybenzylidene}-1,4-diaminobenzene, **16f**; (b) representations of some deduced ^{1}H-^{13}C HMBC correlations 267

Figure 6.27 Photomicrograph of fluid oily streaks in the N* domains upon the heating run prior to N*-I transition (compound **16b**) 272

Figure 6.28 Photomicrograph of N* phase exhibiting violet / blue iridescent colours in formation of oily streaks texture (compound **16d**) 272

Figure 7.1 Condensation reaction between 1,4-diaminobenzene and 3-bromo-4-hydroxybenzaldehyde to yield 4,4’-bis(3-bromo-4-hydroxy-benzylidene)-1,4-diaminobenzene, **17** 274

Figure 7.2 FT-IR spectrum of 4,4’-bis(3-bromo-4-hydroxybenzylidene)-1,4-diaminobenzene, **17** 276

Figure 7.3 Etherification reaction between compound **17** and a series of α,ω-dibromoalkanes to yield 4,4’-bis[3-bromo-4-(*n*-bromoalkyloxy)-benzylidene]-1,4-diaminobenzenes, **18a**-**18h** 277

Figure 7.4 FT-IR spectrum of 4,4’-bis[3-bromo-4-(8-bromooctyloxy)-benzylidene]-1,4-diaminobenzene, **18d** 279

Figure 7.5 FT-IR spectrum of 4,4’-bis[3-bromo-4-(9-bromononyloxy)-benzylidene]-1,4-diaminobenzene, **18e** 280

Figure 7.6 ^{1}H-NMR spectrum of 4,4’-bis[3-bromo-4-(8-bromooctyloxy)-benzylidene]-1,4-diaminobenzene, **18d** 283

Figure 7.7 ^{1}H-NMR spectrum of 4,4’-bis[3-bromo-4-(9-bromononyloxy)-benzylidene]-1,4-diaminobenzene, **18e** 284

Figure 7.8 Etherification reaction between compound **10** and compounds **18a**-**18h** to yield 4,4’-bis{ω-[2-methylbutyl-4’-(4”-phenyl)benzoateoxy]-3-bromo-4-alkyloxybenzylidene}-1,4-diaminobenzenes, **19a**-**19h** 285

Figure 7.9 FT-IR spectrum of 4,4’-bis{ω-[2-methylbutyl-4’-(4”-phenyl)-benzoateoxy]-3-bromo-4-octyloxybenzylidene}-1,4-diaminobenzene, **19d** 288

Figure 7.10 FT-IR spectrum of 4,4’-bis{ω-[2-methylbutyl-4’-(4”-phenyl)-benzoateoxy]-3-bromo-4-nonyloxybenzylidene}-1,4-diaminobenzene, **19e** 289

Figure 7.11 Atom numbering for compound **19d** 290

Figure 7.12 ^{1}H-NMR spectrum of 4,4’-bis{ω-[2-methylbutyl-4’-(4”-phenyl)-benzoateoxy]-3-bromo-4-octyloxybenzylidene}-1,4-diaminobenzene, **19d** 294

Figure 7.13 (a) ^{1}H-^{1}H COSY spectrum of 4,4’-bis{ω-[2-methylbutyl-4’-(4”-phenyl)benzoateoxy]-3-bromo-4-octyloxybenzylidene}-1,4-diaminobenzene, **19d**; (b) representations of some deduced ^{1}H-^{1}H COSY correlations 295

Figure 7.14 ^{13}C-NMR spectrum of 4,4’-bis{ω-[2-methylbutyl-4’-(4”-phenyl)-benzoateoxy]-3-bromo-4-octyloxybenzylidene}-1,4-diaminobenzene, **19d** 296

Figure 7.15 DEPT 90 spectrum of 4,4’-bis{ω-[2-methylbutyl-4’-(4”-phenyl)-benzoateoxy]-3-bromo-4-octyloxybenzylidene}-1,4-diaminobenzene, **19d** 297

Figure 7.16 DEPT 135 spectrum of 4,4’-bis{ω-[2-methylbutyl-4’-(4”-phenyl)-benzoateoxy]-3-bromo-4-octyloxybenzylidene}-1,4-diaminobenzene, **19d** 298

Figure 7.17 (a) ^{1}H-^{13}C HMQC spectrum of 4,4’-bis{ω-[2-methylbutyl-4’-(4”-phenyl)benzoateoxy]-3-bromo-4-octyloxybenzylidene}-1,4-diaminobenzene, **19d**; (b) representations of some deduced ^{1}H-^{13}C HMQC correlations 299

Figure 7.18 (a) ^{1}H-^{13}C HMBC spectrum of 4,4’-bis{ω-[2-methylbutyl-4’-(4”-phenyl)benzoateoxy]-3-bromo-4-octyloxybenzylidene}-1,4-diaminobenzene, **19d**; (b) representations of some deduced ^{1}H-^{13}C HMBC correlations 301

Figure 7.19 Atom numbering for compound **19e** 303

Figure 7.20 ^{1}H-NMR spectrum of 4,4’-bis{ω-[2-methylbutyl-4’-(4”-phenyl)-benzoateoxy]-3-bromo-4-nonyloxybenzylidene}-1,4-diaminobenzene, **19e** 305

Figure 7.21 (a) ^{1}H-^{1}H COSY spectrum of 4,4’-bis{ω-[2-methylbutyl-4’-(4”-phenyl)benzoateoxy]-3-bromo-4-nonyloxybenzylidene}-1,4-diaminobenzene, **19e**; (b) representations of some deduced ^{1}H-^{1}H COSY correlations 306

Figure 7.22 ^{13}C-NMR spectrum of 4,4’-bis{ω-[2-methylbutyl-4’-(4”-phenyl)-benzoateoxy]-3-bromo-4-nonyloxybenzylidene}-1,4-diaminobenzene, **19e** 310

Figure 7.23 DEPT 90 spectrum of 4,4’-bis{ω-[2-methylbutyl-4’-(4”-phenyl)-benzoateoxy]-3-bromo-4-nonyloxybenzylidene}-1,4-diaminobenzene, **19e** 311

Figure 7.24 DEPT 135 spectrum of 4,4’-bis{ω-[2-methylbutyl-4’-(4”-phenyl)-benzoateoxy]-3-bromo-4-nonyloxybenzylidene}-1,4-diaminobenzene, **19e** 312

Figure 7.25 (a) ^{1}H-^{13}C HMQC spectrum of 4,4’-bis{ω-[2-methylbutyl-4’-(4”-phenyl)benzoateoxy]-3-bromo-4-nonyloxybenzylidene}-1,4-diaminobenzene, **19e**; (b) representations of some deduced ^{1}H-^{13}C HMQC correlations 313

Figure 7.26 (a) ^{1}H-^{13}C HMBC spectrum of 4,4’-bis{ω-[2-methylbutyl-4’-(4”-phenyl)benzoateoxy]-3-bromo-4-nonyloxybenzylidene}-1,4-diaminobenzene, **19e**; (b) representations of some deduced ^{1}H-^{13}C HMBC correlations 314

Figure 7.27 Dependence of the transition temperatures on the number of methylene units, *n* in the flexible spacers for compounds **19a**-**19h** 318

Figure 7.28 Dependence of chiral nematic-isotropic transitional entropy, $\Delta S_{N*I}/R$ on the number of methylene units, *n* in the flexible spacers for compounds **19b**-**19f** and **19h** 321

Figure 7.29 N* oily streaks texture of compound **19b** at 170.1 °C upon heating 321

Figure 7.30 Comparison of N*-I transition temperatures among trimers from three series; compounds **13a**-**13h**, **16b**, **16d**, **16f** and **16h** and **19b**-**19f** and **19h** 323

Figure 7.31 Photomicrograph showing the blue phase-N* transition upon cooling of compound **19c** 324

Figure 7.32 DSC trace for compound **19c** with ±5 °Cmin^{-1} heating and cooling rates 324

Figure 8.1 Condensation reaction between 4-hydroxybenzaldehyde and 4-substituted-anilines with terminal Cl or Br atom to yield 4-hydroxy-4’-benzylidenechloroaniline, **22a** and 4-hydroxy-4’-benzylidenebromo-aniline, **22b**, respectively 325

Figure 8.2 FT-IR spectrum of 4-hydroxy-4’-benzylidenebromoaniline, **22b** 326

Figure 8.3 ^{1}H-NMR spectrum of 4-hydroxy-4’-benzylidenebromoaniline, **22b** 327

Figure 8.4 Etherification reaction between compounds **22a**, **22b** and 1,4-dibromo-butane and 1,6-dibromohexane to yield 4-(*n*-bromoalkyloxy)-4’-benzylidene-substituted-anilines, **23a**-**23d** 328

Figure 8.5 FT-IR spectrum of 4-(4-bromobutyloxy)-4’-benzylidenechloroaniline, **23a** 333

Figure 8.6 FT-IR spectrum of 4-(4-bromobutyloxy)-4’-benzylidenebromoaniline, **23c** 334

Figure 8.7 ^{1}H-NMR spectrum of 4-(4-bromobutyloxy)-4’-benzylidenechloroaniline, **23a** 336

Figure 8.8 ^{1}H-NMR spectrum of 4-(4-bromobutyloxy)-4’-benzylidenebromoaniline, **23c** 337

Figure 8.9 Etherification reaction between 2,4-dihydroxybenzaldehyde and compounds **23a**-**23d** to yield benzyl-2,4-oxybis(4’-halogenoanilinebenzylidene-4”-oxy)alkane aldehydes, **24a**-**24d** 338

Figure 8.10 FT-IR spectrum of benzyl-2,4-oxybis(4’-chloroanilinebenzylidene-4”-oxy)butane aldehyde, **24a** 340

Figure 8.11 FT-IR spectrum of benzyl-2,4-oxybis(4’-bromoanilinebenzylidene-4”-oxy)butane aldehyde, **24c** 341

Figure 8.12 ^{1}H-NMR spectrum of benzyl-2,4-oxybis(4’-chloroanilinebenzylidene-4”-oxy)butane aldehyde, **24a** 343

Figure 8.13 ^{1}H-NMR spectrum of benzyl-2,4-oxybis(4’-bromoanilinebenzylidene-4”-oxy)butane aldehyde, **24c** 344

Figure 8.14 Condensation reaction between compounds **24a**-**24d** and corresponding 4-substituted-anilines to yield 4-ethyl- and 4-fluoroanilinebenzylidene-2’,4’-oxybis(4”-halogenoanilinebenzylidene-4”’-oxy)alkanes, **25a**-**25d** and **26a**-**26d** 346

Figure 8.15 FT-IR spectrum of 4-ethylanilinebenzylidene-2’,4’-oxybis(4”-chloroanilinebenzylidene-4”’-oxy)butane, **25a** 349

Figure 8.16 FT-IR spectrum of 4-fluoroanilinebenzylidene-2’,4’-oxybis(4”-bromoanilinebenzylidene-4”’-oxy)butane, **26c** 350

Figure 8.17 Atom numbering for compound **25a** 351

Figure 8.18 ^{1}H-NMR spectrum of 4-ethylanilinebenzylidene-2’,4’-oxybis(4”-chloroanilinebenzylidene-4”’-oxy)butane, **25a** 354

Figure 8.19 (a) ^{1}H-^{1}H COSY spectrum of 4-ethylanilinebenzylidene-2’,4’-oxybis(4”-chloroanilinebenzylidene-4”’-oxy)butane, **25a**;
(b) representations of some deduced ^{1}H-^{1}H COSY correlations 355

Figure 8.20 ^{13}C-NMR spectrum of 4-ethylanilinebenzylidene-2’,4’-oxybis(4”-chloroanilinebenzylidene-4”’-oxy)butane, **25a** 360

Figure 8.21 DEPT 90 spectrum of 4-ethylanilinebenzylidene-2’,4’-oxybis(4”-chloroanilinebenzylidene-4”’-oxy)butane, **25a** 361

Figure 8.22 DEPT 135 spectrum of 4-ethylanilinebenzylidene-2’,4’-oxybis(4”-chloroanilinebenzylidene-4”’-oxy)butane, **25a** 362

Figure 8.23 (a) ^{1}H-^{13}C HMQC spectrum of 4-ethylanilinebenzylidene-2’,4’-oxybis(4”-chloroanilinebenzylidene-4”’-oxy)butane, **25a**; (b) representations of some deduced ^{1}H-^{13}C HMQC correlations 363

Figure 8.24 (a) ^{1}H-^{13}C HMBC spectrum of 4-ethylanilinebenzylidene-2’,4’-oxybis(4”-chloroanilinebenzylidene-4”’-oxy)butane, **25a**; (b) representations of some deduced ^{1}H-^{13}C HMBC correlations 364

Figure 8.25 Atom numbering for compound **26c** 365

Figure 8.26 ^{1}H-NMR spectrum of 4-fluoroanilinebenzylidene-2’,4’-oxybis(4”-bromoanilinebenzylidene-4”’-oxy)butane, **26c** 367

Figure 8.27 (a) ^{1}H-^{1}H COSY spectrum of 4-fluoroanilinebenzylidene-2’,4’-oxybis(4”-bromoanilinebenzylidene-4”’-oxy)butane, **26c**; (b) representations of some deduced ^{1}H-^{1}H COSY correlations 368

Figure 8.28 ^{13}C-NMR spectrum of 4-fluoroanilinebenzylidene-2’,4’-oxybis(4”-bromoanilinebenzylidene-4”’-oxy)butane, **26c** 371

Figure 8.29 DEPT 90 spectrum of 4-fluoroanilinebenzylidene-2’,4’-oxybis(4”-bromoanilinebenzylidene-4”’-oxy)butane, **26c** 372

Figure 8.30 DEPT 135 spectrum of 4-fluoroanilinebenzylidene-2’,4’-oxybis(4”-bromoanilinebenzylidene-4”’-oxy)butane, **26c** 373

Figure 8.31 (a) ^{1}H-^{13}C HMQC spectrum of 4-fluoroanilinebenzylidene-2’,4’-oxybis(4”-bromoanilinebenzylidene-4”’-oxy)butane, **26c**; (b) representations of some deduced ^{1}H-^{13}C HMQC correlations 374

Figure 8.32 (a) ^{1}H-^{13}C HMBC spectrum of 4-fluoroanilinebenzylidene-2’,4’-oxybis(4”-bromoanilinebenzylidene-4”’-oxy)butane, **26c**; (b) representations of some deduced ^{1}H-^{13}C HMBC correlations 376

Figure 8.33 DSC trace of compound **25a** with heat capacity change of 0.4 kJ(mol·°C)$^{-1}$ at 13.4 °C. G indicates the glassy state. The heat capacity change is observed at G-N phase transition upon second heating. 382

Figure 8.34 DSC trace of compound **25b** with heat capacity change of 0.3 kJ(mol·°C)$^{-1}$ at 5.2 °C. G indicates the glassy state. The heat capacity change is observed at G-N phase transition upon second heating. 384

Figure 8.35 Plot of phase temperature (°C) range upon cooling for compounds **24a**-**24d** (* denotes mp) 385

Figure 8.36 Plot of phase temperature (°C) range upon cooling for fluorinated compounds **26a**-**26d** (* denotes mp) 386

Figure 8.37 Powder X-ray diffraction profile for compound **25c** in the nematic phase at 120.0 °C. The red curve indicates that the signal fits the Lorentzian function 389

Figure 8.38 Proposed MM2 optimized structure of **25c** based on minimum energetic parameters. The estimated length of the trimer is 40 Å. 389

Figure 8.39 Nematic schlieren texture with twofold and fourfold brushes of compound **25d** at 117.8 °C upon cooling 391

SINTESIS DAN SIFAT MESOMORFIK BAGI OLIGOMER PELBAGAI-FUNGSIAN BERSIMETRI DAN BUKAN-SIMETRI

ABSTRAK

Enam siri oligomer bersimetri dan tidak bersimetri dengan pelbagai kumpulan berfungsi telah disintesis dan dicirikan. Oligomer ini terdiri daripada dua siri dimer tidak bersimetri, tiga siri trimer bersimetri dan satu siri trimer tidak bersimetri. Siri pertama dimer tidak bersimetri, α-(4-benzilidina-tertukarganti-anilina-4’-oksi)-ω-[2-metilbutil-4’-(4”-fenil)benzoatoksi]alkana terdiri daripada sepuluh homolog yang berbeza dari segi kumpulan tertukarganti, X = H, CH_3, F, Cl and Br dan juga spaser C_6H_{12} and C_8H_{16}. Dimer ini mempamerkan fasa nematik enantiotropik kecuali sebatian dengan X = H. Kedua-dua dimer dengan atom tertukarganti Br juga mempamerkan fasa SmA ‘*intercalated*’. Penyusunan ‘*intercalated*’ ialah hasil daripada, sekurang-kurangnya sebahagiannya, interaksi lebih sesuai antara dua teras mesogenik berbeza. Dimer tidak bersimetri dalam siri kedua iaitu α-(4-benzilidinakloroanilina-4’-oksi)-ω-[(4-(tiofena-2-karboksil)benzilidinaanilina-4’-oksi]-alkana dengan spaser yang terdiri daripada C_5H_{10} sehingga $C_{12}H_{24}$ adalah mesogen enantiotropik. Sifat nematogenik ini menunjukkan tentang pengaruh tarikan terminal antara teras 4-benzilidinakloroanilina dan tiofena-2-karboksilat. Kesan ganjil-genap yang kuat dari segi suhu peralihan nematik-isotropik dimer ini juga telah direkodkan. Dalam siri ketiga oligomer, trimer bersimetri 4,4’-bis{ω-[2-metilbutil-4’-(4”-fenil)benzoatoksi]alkiloksi-benzilidina}-1,4-diaminobenzena adalah nematogen dan smektogen kiral. Selain daripada fasa nematik kiral, setiap homolog dalam siri ini juga mempamerkan fasa SmA secara enantiotropik. Fasa SmC kiral feroelektrik juga diperhatikan untuk homolog dengan spaser daripada C_5H_{10} sehingga C_9H_{18}. Tambahannya, ahli-ahli ganjil mempamerkan fasa biru dan fasa smektik bertertib-tinggi. Dua lagi siri trimer dengan kumpulan tertukarganti lateral iaitu 4,4’-bis{ω-[2-metilbutil-4’-(4”-fenil)benzoatoksi]-3-metoksi-4-alkiloksibenzilidina}-1,4-

diaminobenzena dan 4,4’-bis{ω-[2-metilbutil-4’-(4”-fenil)benzoatoksi]-3-bromo-4-alkiloksibenzilidina}-1,4-diaminobenzena telah disediakan. Dengan kehadiran kumpulan metoksi lateral, empat trimer genap mempamerkan fasa nematik kiral enantiotropik sementara ahli ganjil tidak bersifat mesogenik. Sementara itu, setiap trimer tertukarganti-Br dalam siri mempamerkan fasa nematik kiral enantiotropik kecuali trimer dengan spaser C_5H_{10} dan $C_{11}H_{22}$. Sementara trimer C_5H_{10} tidak mesogenik, ahli dengan $C_{11}H_{22}$ mempamerkan fasa nematik kiral monotropik. Trimer dengan spaser C_7H_{14} dan C_9H_{18} juga menunjukkan fasa biru. Kestabilan terma yang rendah dan sifat nematogenik trimer dengan kumpulan tertukarganti lateral adalah hasil daripada halangan lateral untuk interaksi antara-molekul. Dalam siri keenam oligomer, trimer tidak bersimetri 4-etil- dan 4-floroanilinabenzilidina-2’,4’-oksibis(4”-halogenoanilinabenzilidina-4”’-oksi)alkana mengandungi sama ada atom klorin atau bromin terminal. Trimer ini juga berbeza antara satu sama lain daripada segi spaser C_4H_8 and C_6H_{12}. Trimer ini adalah nematogenik dengan suhu peralihan yang rendah disebabkan arkitektur molekul bercabang. Tiga daripada homolog dengan kumpulan etil juga merupakan nematogen kekacaan dengan suhu peralihan kaca kurang daripada 15°C.

SYNTHESIS AND MESOMORPHIC PROPERTIES OF SYMMETRIC AND NON-SYMMETRIC MULTI-FUNCTIONALIZED OLIGOMERS

ABSTRACT

Six series of novel symmetric and non-symmetric oligomers with multi-functional groups have been synthesized and characterized. The oligomers comprise two series of non-symmetric dimers, three series of symmetric trimers and one series of non-symmetric trimers. The first series of non-symmetric dimers, α-(4-benzylidene-substituted-aniline-4’-oxy)-ω-[2-methylbutyl-4’-(4”-phenyl)benzoateoxy]alkanes consists of ten homologues varying in terms of terminal substituents, X = H, CH_3, F, Cl and Br as well as C_6H_{12} and C_8H_{16} spacers. The dimers exhibit the enantiotropic nematic phase except compounds with X = H. Both Br-substituted dimers also exhibit the intercalated SmA phase. The intercalated arrangement is the result, at least in part, of the more favourable interaction between the two unlike cores. The non-symmetric dimers in the second series, α-(4-benzylidenechloroaniline-4’-oxy)-ω-[4-(thiophene-2-carboxyl)benzylideneaniline-4’-oxy]alkanes with spacers ranging from C_5H_{10} to $C_{12}H_{24}$ are all enantiotropic mesogens. The nematogenic properties indicate the predominant terminal attraction between the 4-benzylidenechloroaniline and thiophene-2-carboxylate cores. Strong odd-even effect in terms of the nematic-isotropic transition temperatures of the dimers has also been recorded. In the third series of oligomers, the symmetric trimeric 4,4’-bis{ω-[2-methylbutyl-4’-(4”-phenyl)benzoateoxy]alkyloxy-benzylidene}-1,4-diaminobenzenes are chiral nematogens and smectogens. Apart from the chiral nematic phase, every homologue in this series also exhibits the SmA phase enantiotropically. The chiral SmC phase is also observed for the homologues with spacers from C_5H_{10} to C_9H_{18}. Additionally, the odd members exhibit the blue phase and monotropic high-order smectic phase. Another two series of trimers with lateral substituents namely the 4,4’-bis{ω-[2-methylbutyl-4’-(4”-phenyl)benzoateoxy]-3-methoxy-4-alkyloxybenzylidene}-

1,4-diaminobenzenes and 4,4’-bis{ω-[2-methylbutyl-4’-(4”-phenyl)benzoateoxy]-3-bromo-4-alkyloxybenzylidene}-1,4-diaminobenzenes have been prepared. With the presence of lateral methoxy groups, the four even trimers exhibit the enantiotropic chiral nematic phase whilst the odd members are not mesogenic. On the other hand, every Br-substituted trimer in the series exhibits the enantiotropic chiral nematic phase except the trimers with C_5H_{10} and $C_{11}H_{22}$ spacers. Whilst the C_5H_{10} trimer is not mesogenic, the member with $C_{11}H_{22}$ spacers exhibits the monotropic chiral nematic phase. The trimers with C_7H_{14} and C_9H_{18} spacers also show the blue phase. The lower phase thermal stability and nematogenic behaviour of the trimers with lateral substituents is the result of lateral hindrance for intermolecular interaction. In the sixth series of oligomers, the non-symmetric trimeric 4-ethyl- and 4-fluoroanilinebenzylidene-2’,4’-oxybis(4”-halogenoanilinebenzylidene-4”’-oxy)alkanes incorporate either a terminal chlorine or bromine atom. The trimers also vary from each other in terms of C_4H_8 and C_6H_{12} spacers. The trimers are nematogenic with low transition temperatures due to the branched molecular architecture. Three of the members with ethyl group are also glassy nematogens with glass transition temperatures less than 15°C.

1.0 INTRODUCTION

1.1 Liquid crystals: History

Liquid crystals are fascinating materials which have been utilized in many types of applications such as display devices. The first liquid crystal compound named cholesteryl benzoate was found in 1888 by F. Reinitzer (Kelker and Hatz, 1980). His initial observation uncovered that the compound possessed two distinctive phase transitions at 146.6 °C and 180.6 °C, respectively. The substance exhibited iridescent colours in between these transition temperatures which were characteristic of a state later known as liquid crystal. By the 20th century, the correlating principles of liquid crystals and molecular structures had been developed by D. Vorländer. In general, as cited by Kelker and Hatz, the terminology of liquid crystals accepted today is based on the original work by G. Friedel. His pioneering work via polarizing microscopic observation introduced the terms such as nematic and smectic phases which have been used widely until today.

1.2 Liquid crystals: Concept

Liquid crystal is known as the fourth state of matters besides solid, liquid and gas. As shown in figure 1.1, liquid crystal is an intermediate phase between a crystal and a liquid. It is important to mention that, in relative terms, only a small percentage of chemical compounds possess liquid crystalline properties. Most substances known today have only two phase transitions with respect to the increase of temperature. The two transitions are melting and boiling. However, a liquid crystal is different from conventional compounds as it has at least another phase transition to the liquid crystalline phase from the crystalline phase before clearing to the isotropic liquid.

For discussion on liquid crystals, the liquid-gas transition is not of interest because in the gas phase, molecules are in total random motion and do not possess any degree of ordering. The difference between these two phases is the molecules of a gas is widely separated from one another and move in a path largely unaffected by intermolecular forces.

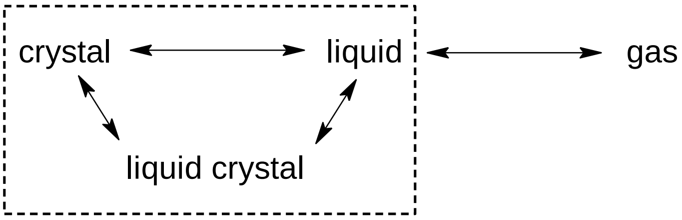

Figure 1.1: Primary phase transitions and phase transitions involving liquid crystalline phase (in dotted box)

1.3 Mesophases

The liquid crystalline phase is known as mesophase. There are many mesophases which have been discovered but these phases can be categorized into two major ones; nematic and smectic phases. The nematic phase is exhibited at higher temperature in comparison to the smectic phase. The nematic phase has more similarities to the liquid phase whilst the smectic and crystal phase are more similar to each other.

1.3.1 Nematic phase

In the nematic phase, the molecules possess some degree of orientational order. In average, the molecules are all aligned towards similar direction in the nematic phase. The orientational direction is represented by the director (figure 1.2). There is no positional ordering in the nematic phase.

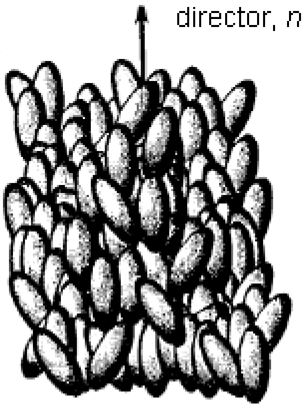

Figure 1.2: Nematic phase (Barón, 2001)

1.3.1.1 Chiral nematic phase

The chiral nematic phase is also known as the cholesteric phase. In the chiral nematic phase, the chiral center of every molecule provides intermolecular force which enables molecules to align at a slight angle from one another. This leads to a stack of nematic layers with the local director in each layer twisted around a single axis as illustrated in figure 1.3. The overall molecular orientation in the chiral nematic phase is visualized as a continuous twisting pattern like a helix from one layer to another.

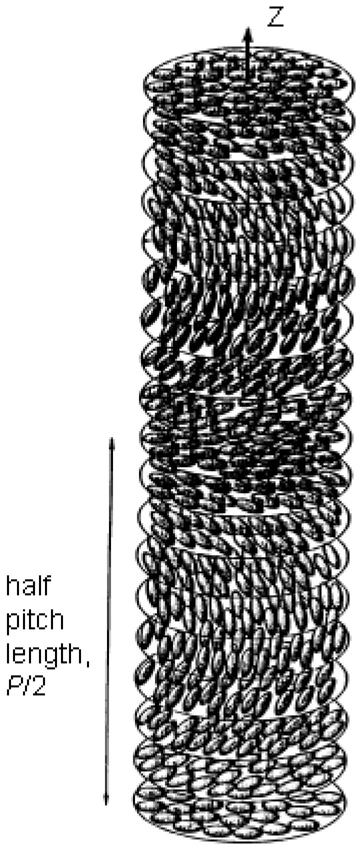

Figure 1.3: Chiral nematic phase (Barón, 2001)

1.3.2 Smectic phase

Unlike the nematic phase, the smectic phase possesses some similarities to the crystal phase as the smectic molecules are arranged in layer-like ordering. In other words, there exist positional orders in a smectic phase. In the smectic phase, the molecules also possess orientational order which is similar to that of a nematic phase.

1.3.2.1 Non-chiral smectic phase

Based on the differences in molecular orientation and packing in the smectic layers, more than ten different smectic modifications have been reported. The simplest smectic phase is known as the smectic A (SmA) phase. In the SmA phase, molecules are aligned perpendicular to the smectic plane as shown in figure 1.4(a). In the layers, molecules do not have any particular positional order. The SmA phase has been observed in various liquid crystalline compounds such as the 5,5’-substituted-2,2’-bipyridines with flexible alkoxy terminals (Douce *et al*., 1996).

The SmA phase can be further classified into different types such as the monolayer, bilayer, interdigitated and intercalated SmA phase. The monolayer SmA phase (SmA_1) is the simplest SmA phase and is the most frequently encountered SmA phase. The SmA_1 layer thickness corresponds to the length of the molecule. Bilayer SmA (SmA_2) phase with layer spacing twice the molecular length is usually observed for liquid crystals with a terminal dipolar group such as cyano or nitro group. This is due to the electrostatic interaction arising from the opposite direction of longitudinal component with regard to the cyano or nitro dipoles (Madhusudana, 2001). In the interdigitated SmA (SmA_d) phase, the layer thickness is more than the length of one molecule but less than the length of two molecules. The SmA_d phase is usually observed for liquid crystals with two different mesogenic cores in the molecular structure. The driving force for this phase is however not confined to only the presence of two unlike cores in the structure, as electrostatic interaction between certain groups like the polar and polarizable cyanobiphenylyl groups is known to play a key role in inducing interdigitation. The length of the terminal flexible chain is also important in the sense that if the chain length is more than the length of the flexible core, the long terminal chain cannot be accommodated in the available space leading to the formation of interdigitation (Attard *et al.,* 1994). Contrary to SmA_d, the smectic layer periodicity in the intercalated SmA (SmA_c) phase is approximately half the molecular length. The intercalation, which often occur among the non-symmetric dimers, results from a specific interaction between the unlike mesogenic cores enhanced by an entropy gain resulting from the uniform mixing of such groups (Blatch *et al.,* 1997). The observations of SmA_c phase for symmetric dimers is less common, but nevertheless, it has also been reported for the symmetric dimers incorporating two biphenyl groups with terminal OC_4H_9 groups. The intercalated smectic phase is possibly driven by an interaction between the carbonyl groups which link the spacer to the mesogenic units and the ether groups which connect the terminal chains to the mesogenic moieties (Attard *et al.*, 1994 and Watanabe *et al.*, 1993).

The smectic C (SmC) phase is the tilted analogue of the SmA phase. In each SmC layer, molecules are arranged in similar order as in SmA phase. However, as illustrated in figure 1.4(b), in every SmC layer, molecules are tilted at a constant tilt angle (θ) with respect to the layer normal. From X-ray diffraction analyses, reports have shown that for a number of liquid crystal materials, the θ in the SmC phase is temperature dependent. In other words, the θ of the SmC molecules may increase or decrease with respect to the changing of temperature.

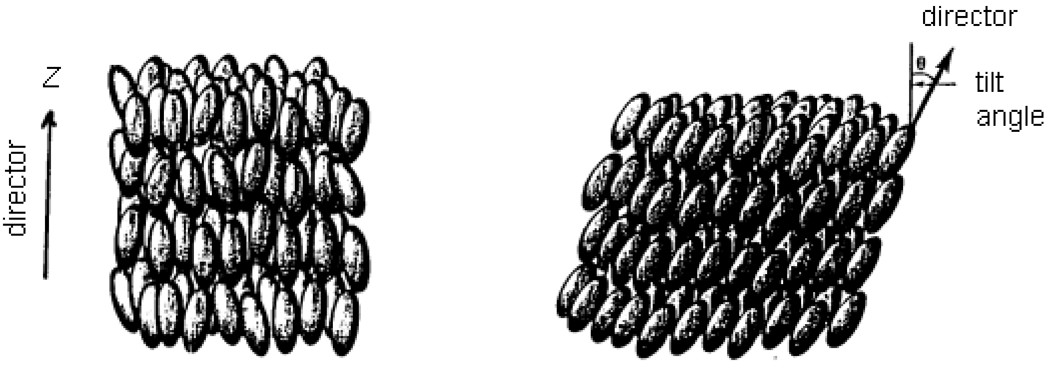

(a) (b)

Figure 1.4: Molecular arrangement in (a) SmA phase with *Z* = optic axis; (b) SmC phase (Barón, 2001)

Apart from the SmA and the SmC phases of which the layers are unstructured, the hexatic smectic phases namely the SmB, SmF and SmI phases have also been observed. In the SmB phase, the director is perpendicular to the layers with long-range hexagonal bond-orientational order. The bond-orientational order represents the long range orientational but short range positional ordering of molecules within a smectic layer (Dierking, 2003). The illustration of the molecular organization in a SmB phase is given in figure 1.5.

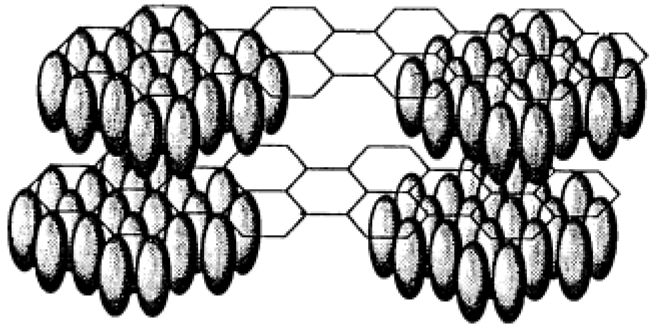

Figure 1.5: SmB phase (Barón, 2001)

Contrary to the SmB phase, the director in the SmF and SmI phases is tilted with respect to the layer normals. For the SmF phase, the director is tilted towards the side of the hexagons as shown in figure 1.6(a). On the other hand, the molecules in the SmI phase tilt towards the apex of the hexagon (figure 1.6(b)). The in-plane positional correlations in the SmI phase are slightly greater than in the SmF phase.

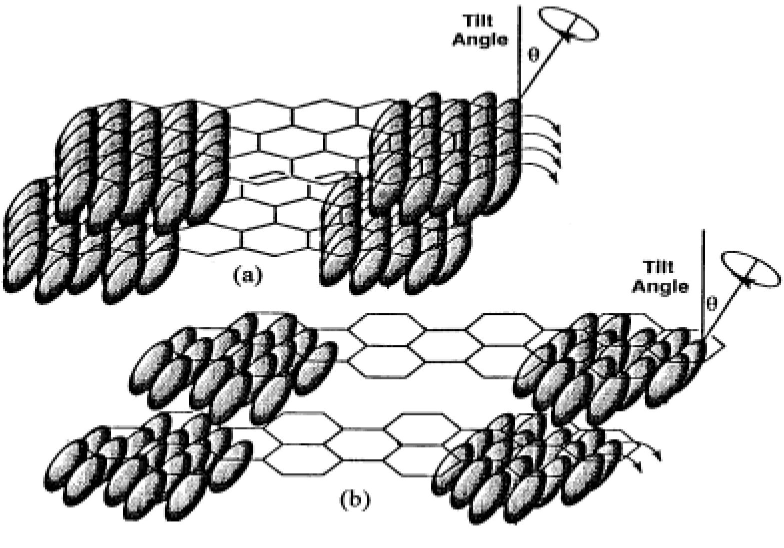

Figure 1.6: Illustration of the respective tilt directions of the director in the (a) SmF; (b) SmI phases

1.3.2.2 Chiral smectic phase

The chiral smectic C (SmC*) phase is one of the most widely discussed chiral smectic phases (Lunkwitz *et al.,* 1998 and Hamaneh and Taylor, 2005). A host of materials exhibiting the SmC* phase have been synthesized such as the mesogenic derivatives of 2S,3S-2-halogeno-3-methylpentanoic acid (Szydłowska *et al.,* 1999). In the similar manner to SmC phase, in every layer molecules are tilted at a constant tilt angle with respect to the axis perpendicular to the plane. In addition to this, the SmC* molecules are arranged in a macroscopic helical pattern as the result of precession of the tilt about the same axis from one layer to another (figure 1.7). For a particular material, the rotation always occurs in the same direction whether it is left-handed or right-handed (Singh, 2002).

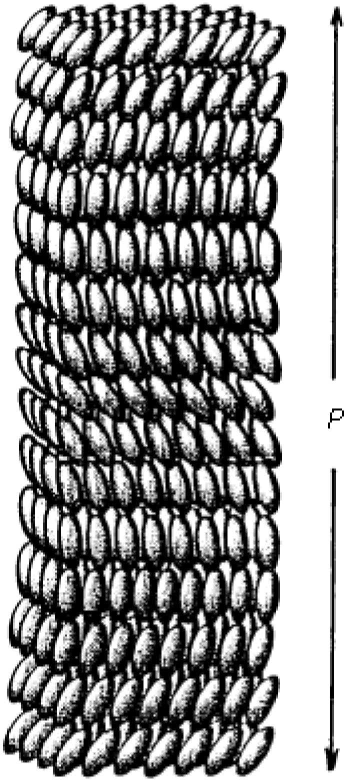

Figure 1.7: SmC* phase with *P* = helical pitch (Barón, 2001)

1.3.2.3 Unidentified smectic phase

Irrespective of whether the liquid crystals are optically active or not, there have been few cases whereby a smectic phase cannot be determined conclusively by powder X-ray diffraction, mesophase texture observation and even miscibility studies. In such cases, the smectic phase is often called as smectic X (SmX) which represents an unidentified smectic phase. One such example is exhibited by the five-ring λ-shaped mesogenic compounds of which three unidentified smectic phases have been observed (Yamaguchi *et al.,* 2005). Another example of unidentified smectic phase has also been discussed for a laterally fluorinated banana-shaped liquid crystal (Lee *et al.,* 2001).

1.3.3 Blue phase

The blue phase is often observed in between the chiral nematic phase and the isotropic phase. In terms of structure, the blue phase possesses three-dimensional spatial distribution of helical director axes leading to a frustrated structure as shown in figure 1.8 (Meiboom *et al.,* 1981 and Barón, 2001). Within every double twist cylinder, the local director rotates around any given radius of the cylinder. At the core of the cylinder, the director is oriented parallel to the cylinder long axis. On moving outwards, the local director twists along any radius until the twist angle is approximately 45° at the edge of the double twist cylinder. The blue phase only exists in chiral liquid crystalline materials with smaller helical pitch (Stegemeyer, 1999). This characteristic has been reported for the non-symmetric dimers with odd parity of which the pitch is smaller in comparison to the even counterparts (Blatch *et al.,* 1997). Other examples of liquid crystals which have also exhibited the blue phase are the three-ring terephthalates with four ester linkages (Fodor-Csorba *et al.,* 1998).

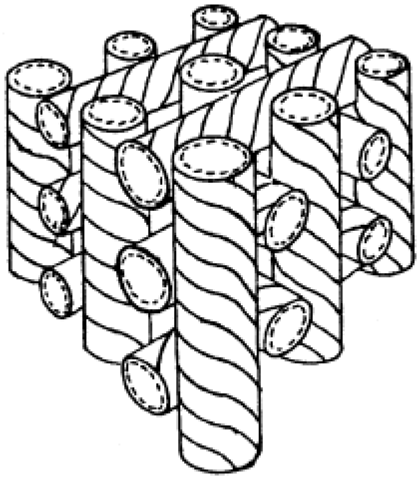

Figure 1.8: A blue phase model consisting of double-twist cylinders forming a cubic lattice (Barón, 2001)

1.4 Mesogen

A mesogen is a compound which can exist as a liquid crystal phase under suitable conditions of pressure, temperature and concentration. Based on the aspect of molecular structure, mesogens can be divided to several types including the calamitic, discotic, banana-shaped, laterally branched and oligomeric systems.

1.4.1 Calamitic mesogens

Calamitic mesogens are also known as rod-like mesogens due to the linearity of the molecular structure. As such, majority of calamitic mesogens involves *para-para* aromatic substitutions to give the rod-like structures. Calamitic mesogens possess high shape anisotropy which are favourable for layered molecular arrangement in the mesophase. Two examples of calamitic mesogens are shown in figure 1.9(a) and (b).

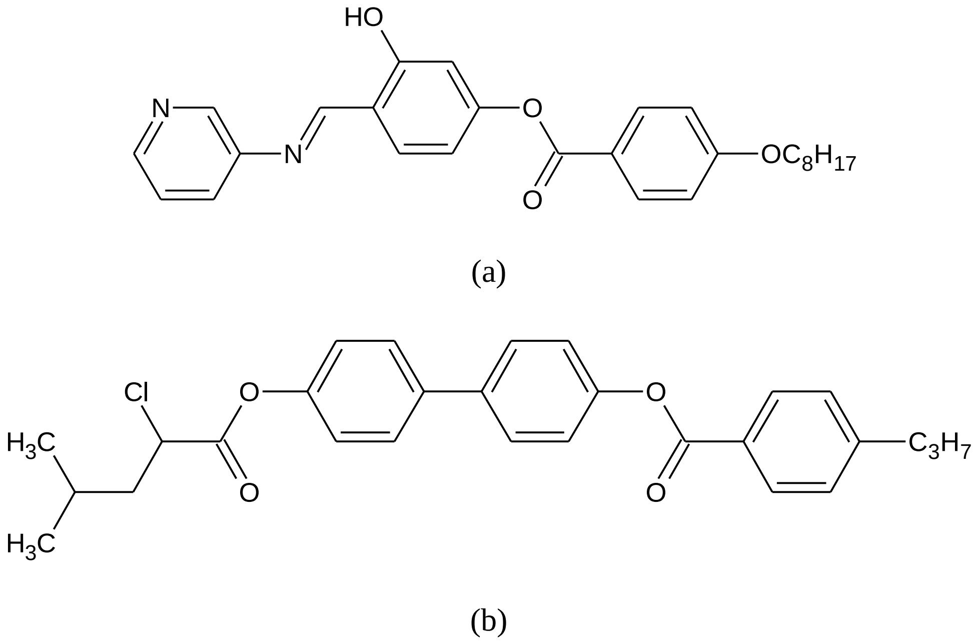

Figure 1.9: Two examples of calamitic mesogens (a) N-[4-(4-octyloxybenzoyloxy)-2-hydroxybenzylidene]-3-aminopyridine (Takase *et al.*, 2003); (b) 4-[(S)-2-chloro-4-methylpentanoyloxy]-4'-[4-propylbenzoyloxy]biphenyl (Schacht *et al.*, 1998)

1.4.2 Discotic mesogens

Discotic mesogens are mesogens with disc- or sheet-shaped structures. The mesophases formed by columnar stacking of discotic mesogens are called the columnar mesophases. An example of discotic mesogen is shown in figure 1.10.

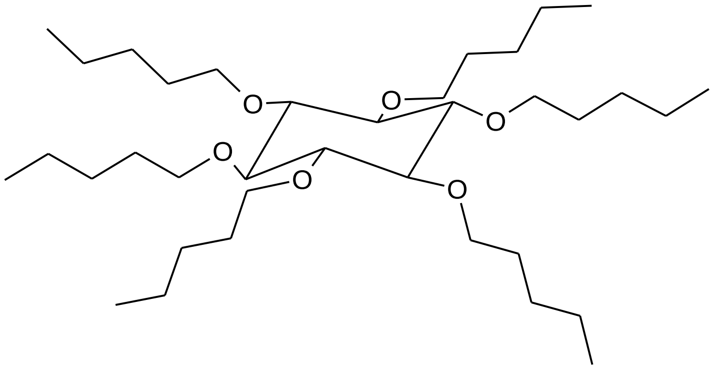

Figure 1.10: Inositol ether (Tschierske, 1998)

1.4.3 Banana-shaped mesogens

Banana-shaped mesogens possess the bent molecular structure due to the 1,3-aromatic substitution at the center of the rigid mesogenic core. Due to the unique bent structure, banana-shaped liquid crystals exhibit unconventional mesophases such as the B_6 mesophase and few chiral mesophases even if the molecules do not contain any chiral centers. An example of banana-shaped liquid crystals is 4,6-dichloro-1,3-phenylenebis[4-(4-*n*-octyloxyphenyliminomethyl)benzoate] with the molecular structure as shown in figure 1.11 (Lee *et al.*, 2003).

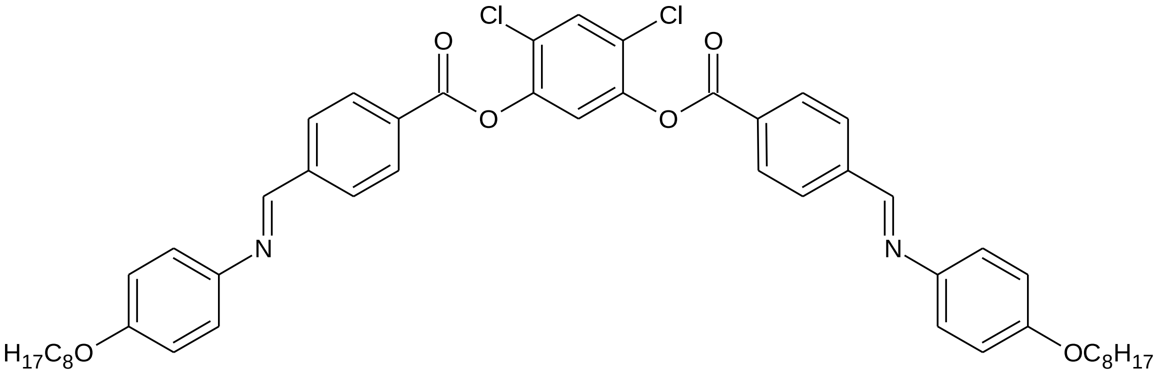

Figure 1.11: 4,6-Dichloro-1,3-phenylenebis[4-(4-*n*-octyloxyphenyliminomethyl)-benzoate] (Lee *et al.*, 2003)

1.4.4 Laterally branched mesogens

An alkyl or aromatic group can be introduced to a calamitic mesogen at a lateral position to form the laterally branched mesogen. Until 1983, it was generally accepted that a lateral substituent would diminish the liquid crystalline properties with the extent of the effect depending on the size of substituent. However, in 1983 and 1984, it was then found that compounds with large flexible lateral substituents are also mesogenic as well (Vora and Prajapati, 2002). Since then, a host of novel compounds with different type of lateral substituents have been reported. The molecular structure for one of these compounds is shown in figure 1.12. However, vast majority of these reported laterally branched mesogens are monomeric, e.g. not oligomeric, in terms of molecular constitution. As such, the mesogenic group is present as one interconnected unit as a whole with the flexible alkyl groups either attached at the terminals or as lateral substituent itself.

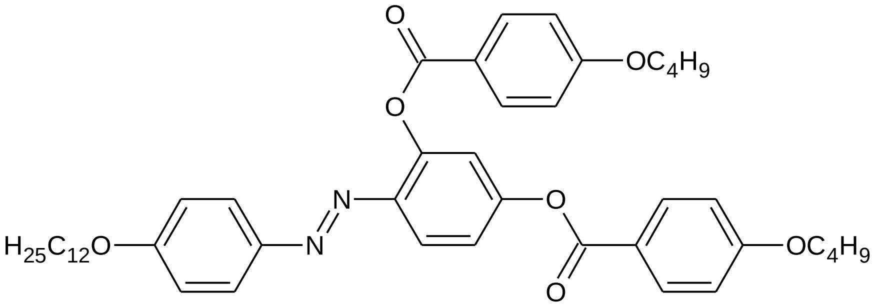

Figure 1.12: 4-Dodecyloxy-2’-(4-butoxybenzoyloxy)-4’-(4-butoxybenzoyloxy)-azobenzenes (Berdagué *et al*., 1993)

1.4.5 Oligomeric mesogens

Oligomeric mesogens have been given considerable amount of attention as these compounds are used as models for the semi-flexible main chain liquid crystal polymers (Imrie and Henderson, 2002 and Pal *et al.*, 2007). The shortest liquid crystal oligomer, the dimer consists of two mesogenic units connected by one flexible group called the spacer in every molecule. A symmetric dimer possesses two identical mesogenic fragments. However, the mesogenic units may not be necessarily the same to each other. In the case where the mesogenic units are different from each other, non-symmetric liquid crystal dimers are formed. The examples of symmetric and non-symmetric dimers are shown in figure 1.13(a) and (b), respectively.

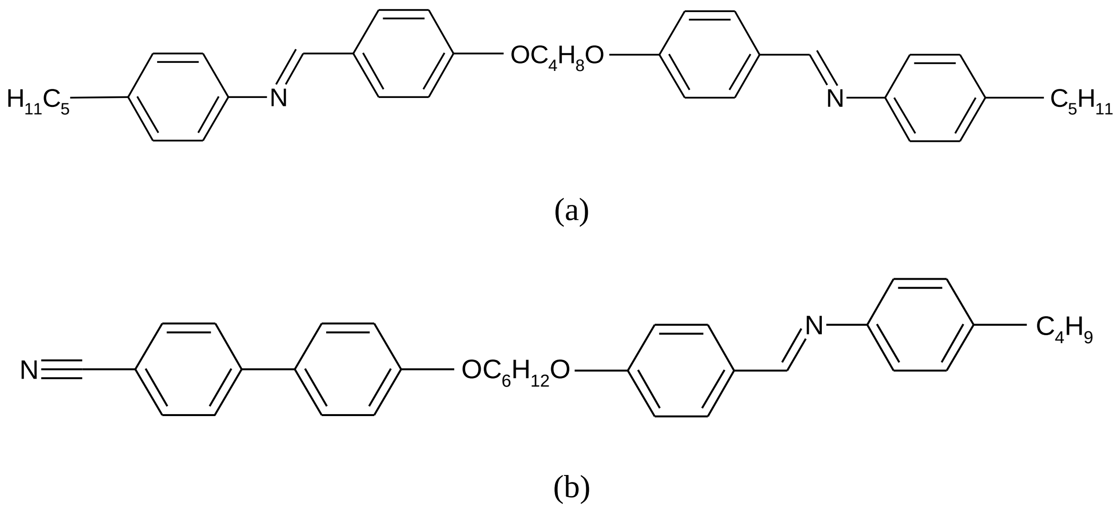

Figure 1.13: Respective example of symmetric dimer and non-symmetric dimer (a) α,ω-bis(4-pentylanilinebenzylidene-4’-oxy)butane (Date *et al*., 1992); (b) α-(4-cyanobiphenyl-4’-oxy)-ω-(4-butylanilinebenzylidene-4’-oxy)-hexane (Hogan *et al*., 1988)

Recently, another series of non-symmetric dimers have been reported, of which the dimers contain cholesterol and 4-(*trans*-4-*n*-hexylcyclohexyl)benzoic acid moieties linked with the central spacer through two ester bonds (Yu *et al.*, 2008). The general structure of the dimer is given in figure 1.14.

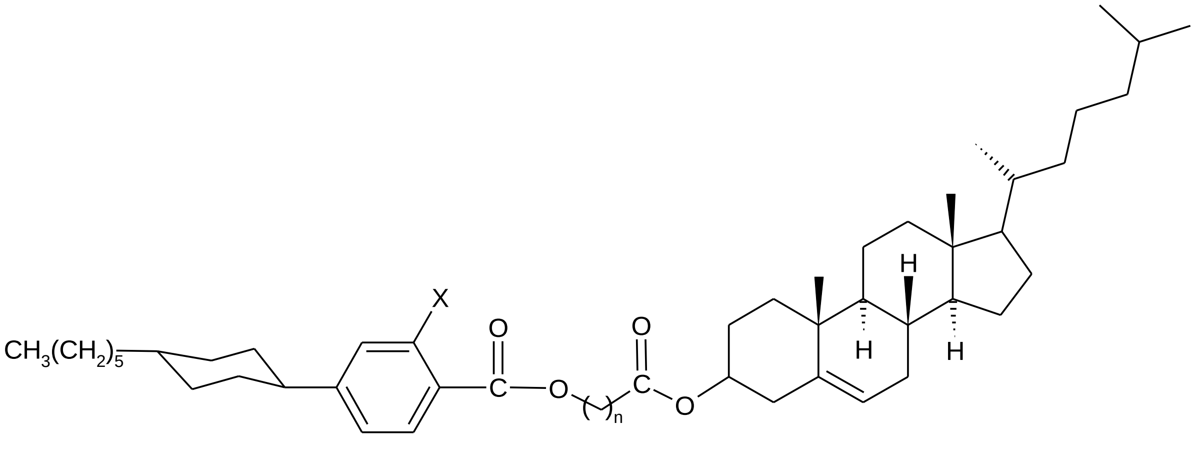

Figure 1.14: Structure for the dimer which contains cholesterol and 4-(*trans*-4-*n*-hexylcyclohexyl)benzoic acid moieties (Yu *et al.*, 2008)

The trimeric liquid crystals contain three mesogenic cores separated by two flexible spacers in every molecule. In a similar manner to liquid crystal dimers, the trimers can be non-symmetric as well. For trimers, the asymmetry can be introduced to the structure by incorporating two spacers with different number of methylene units or two different mesogenic cores. A trimer can also be non-symmetric by having an asymmetric central core despite having both terminals identical to each other. The examples of symmetric and non-symmetric trimers are depicted in figure 1.15(a) and (b), respectively.

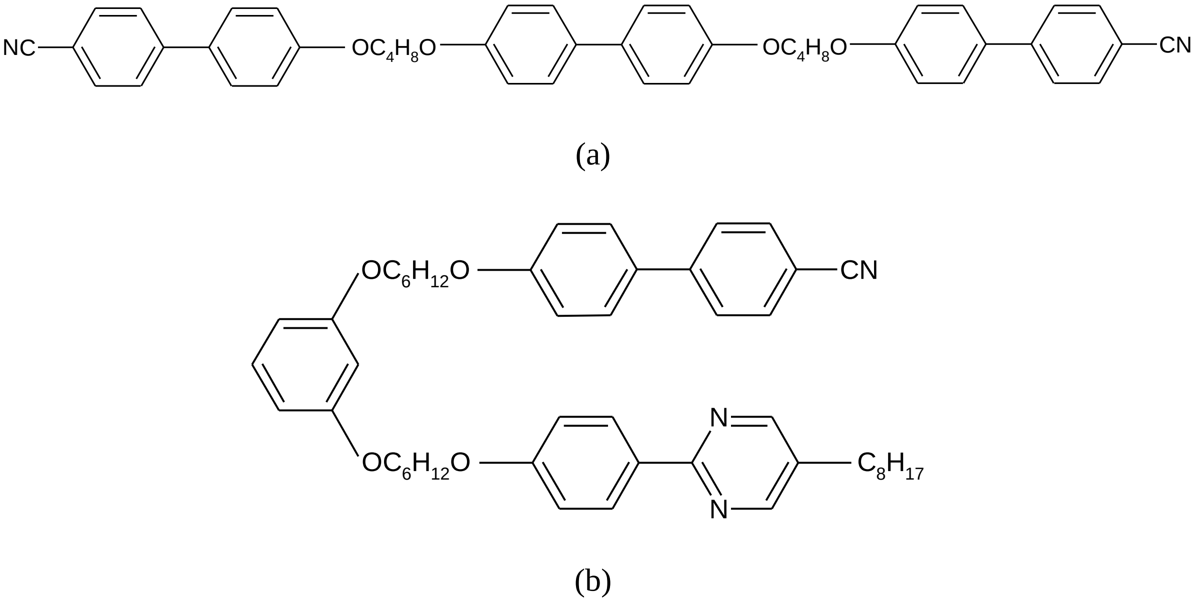

Figure 1.15: Respective example of symmetric trimer and non-symmetric trimer
(a) 4,4’-bis[ω-(4-cyanobiphenyl-4’-yloxy)butyloxy]biphenyl;
(b) mesogen incorporating 5-octylpyrimidine-2-yl and 4-cyanophenyl moieties (Yoshizawa *et al.*, 2005)

1.5 Structure-property relationship of liquid crystals

The liquid crystalline properties of mesogenic compounds are governed by the molecular structures and the attributes as the result of these structures. It is known that by substituting certain atom or group of atoms in a molecule, the liquid crystalline properties may also be altered. The correlation between chemical constitution and liquid crystalline properties of which is available today is largely based on the early work by D. Vorländer, C. Weygand, C. Wiegand and G. W. Gray (Kelker and Hatz, 1980). The general criteria in order for molecules to be mesogenic are as follow:

a) The most favourable geometry of liquid crystal molecules is rod-like and narrow reflecting high shape anisotropy.

b) The molecules possess high anisotropy of polarizability.

c) The melting point of the compound must not be too high.

d) Permanent dipolar groups are present in the molecules.

1.5.1 Structure-property relationship of liquid crystal oligomers

1.5.1.1 The influence of spacer length and parity on the liquid crystalline properties of oligomers

Previous researches have shown that the liquid crystalline properties of oligomeric mesogens are strongly dependent on the length and parity of the flexible spacers, in a manner strongly reminiscent of that seen for the semi-flexible main chain liquid crystalline polymers (Henderson and Imrie, 2005). In a homologous series for instance, the dimers and trimers with shorter spacers may exhibit liquid crystalline properties which differs from those observed for the longer counterparts. One of such unique characteristics which have been noted for the symmetric dimers is the decreasing tendency to exhibit smectogenic properties upon increasing spacer length (Date *et al.*, 1992).

In general, the dependence of transition temperatures of oligomers upon substituting the spacers with different number of methylene units, *n* can be observed as the zigzag alternation pattern of which the temperature is often lower for the homologues with odd-parity spacers. For example, in a series of eight-ring tetramers with two azo and two Schiff base linkages, the melting points exhibited pronounced alternation as *n* was increased although attenuation was not observed upon ascending this series (Henderson and Imrie, 2005). The behaviour is explained by the change in conformational statistical weights of the spacer on melting into a nematic phase is small for an even-parity spacer but large for an odd-parity spacer. This behaviour may also reflects that the tetramers with even spacers which presumably adopt more elongated conformations, pack more efficiently into a crystal lattice than the odd counterparts, which adopt, on average, bent molecular shapes.

1.5.1.2 The influence of unlike cores and non-symmetric structures on the liquid crystalline properties of oligomers

The non-symmetric oligomers exhibit liquid crystalline properties differently from the oligomers with symmetric molecular architectures. In recent years, the non-symmetric oligomers have been increasingly given attention by researchers to understand how these non-symmetric molecules interact with each other especially to exhibit smectic phases with untypical layer periodicities. One of such examples is the α-(4-cyanobiphenyl-4’-yloxy)-ω-[4-(5-alkylpyrimidine-2-yl)phenyl-4”-oxy]alkanes of which the observed smectic phases are either intercalated or interdigitated in nature (Yoshizawa *et al.,* 2006). The details on the intercalated and interdigitated smectic phases have been described in section 1.3.2.1.

1.5.2 Chirality effect on liquid crystalline properties

Chirality is an inherent property of many natural systems such as DNA and enzymes. In liquid crystals, chirality can be introduced in several different ways. It can be introduced within the mesogen by incorporation of chiral centers. Another way which is more commonly practiced in producing materials for applications is the addition of chiral dopant to an achiral host phase (Dierking, 2003).

The presence of one or several chiral centers in a mesogen can tremendously modify the organization of the mesophases (Pansu, 2003). For instance, novel structures like the helical superstructures of the N* and SmC* phases can be induced. The physical properties of mesophases are modified by the loss of mirror symmetry. Tilted chiral smectic phases can exhibit spontaneous polarization and thus these mesophases are pyroelectric (Dierking, 2003).

1.6 Application of liquid crystals

Liquid crystals have been widely used in many high-tech applications such as displays. Liquid crystal displays have dominated the flat panel technology in products such as LCD television and personal digital assistant (PDA). A flat display typically contains a thin layer of liquid crystalline mixture in between two extremely thin glass plates with transparent electrodes twisted by 90° from each other. Polarizing filters are positioned at the outside of the plates whilst the colour filter, transparent electrodes and orientation layers are situated at the inside. The first polarizing filter only allows light of only a particular plane of oscillation to pass through it and subsequently reaches the liquid crystals. The applied voltage orients the molecules perpendicular to the glass plates. The light follows this new orientation and unable to pass through the second filter which is at 90° to the first filter. Therefore the pixel is black. By removing the voltage, the molecules return to the original twisted arrangement. The light follows this twist and is now able to traverse the second filter to give a bright pixel. A liquid crystal display contains million of pixels. The bright and dark pixels produce a pattern which gives the desired image.

Apart from liquid crystal displays, the natural characteristics of liquid crystalline phases have also been exploited for the development of other technological applications. For instance, the helical structures in the chiral smectic C and chiral nematic phases have been recognized for their use in electro-optic and thermochromic devices, respectively (Hemine *et al.,* 2007 and Yelamaggad and Shanker, 2008). Besides, the electroclinic property of the orthogonal layered phase, the chiral smectic A phase holds great promise in spatial light modulation applications (Yelamaggad and Shanker, 2008).

Whilst the monomeric form of liquid crystals have been widely used in various technological devices, the application of the liquid crystalline oligomers mainly lies in serving as a research model for the industrially important semi-flexible main chain liquid crystalline polymers. This is possible due to the similarities in terms of liquid crystalline transitional properties between the oligomers and polymeric systems based on previous findings (Attard *et al.,* 1994 and Imrie and Luckhurst, 1998). In the industries, the liquid crystalline polymers are utilized in the production of high strength fibers. Compared to other polymers, liquid crystalline polymers are advantageous as these materials possess outstanding properties such as high resistance to extreme weathers, radiation, burning and almost all chemicals. Such characteristics of liquid crystalline polymers make them highly suitable to replace other conventionally used materials including metals. The type of liquid crystalline polymers produced is dependent on the incorporated functional groups, for example, terephthalic acid and 4-hydroxybenzoic acid. The concept in the making of these high-strength materials firstly involves the orientation of the polymers in the desired liquid crystalline phase and subsequently quenching to produce highly ordered solid.

1.7 Objectives of the research

The unique relationship between chemical constitution of liquid crystals and the induced mesomorphic characteristics has made the syntheses of novel mesogens an exciting area of research. Over the years, through rigorous investigations, many significant and interesting findings have been reported including:

a) Intercalated and interdigitated smectic phases
b) Reentrant mesophases (Pal *et al.,* 2007)
c) Host of chiral mesophases including the ferroelectric SmC* phase (Liao *et al.,* 2006)
d) Mesogens with unconventional shapes such as H and λ shapes

These findings have deepened our understanding on liquid crystals as well as triggered the keenness in many researchers, including myself, to explore further. In addition to the numerous interesting findings on liquid crystals in general, the unconventional liquid crystalline properties of oligomers have also been inspirational leading to our preparation of six series of novel dimers and trimers incorporating various mesogenic groups. In the Liquid Crystal Research Laboratory, my PhD research project was conducted based on these six objectives:

a) To synthesize a host of new liquid crystal dimers and trimers which are symmetric and non-symmetric in terms of molecular architecture

b) To study the molecular organization of the dimeric and trimeric molecules in the nematic and smectic phase and how structural asymmetry may influence the molecular arrangement and induce unconventional mesophases

c) To investigate the impact of chirality on liquid crystalline properties of trimers

d) To uncover how different substituents at certain positions in the mesogenic fragment can influence the liquid crystalline properties as well as mesophase thermal stability

e) To make comparison and extend our research findings on the novel dimers and trimers in terms of spacer dependent odd-even effect to the polymeric system

f) To study the impact of lateral branching on the trimers in terms of presence or absence of certain mesophases and suppression in transition temperatures

2.0 EXPERIMENTAL

2.1 Chemicals

The fine chemicals used for the syntheses of compounds were purchased from major companies including Merck, Acros Organics, Sigma-Aldrich, Fluka and Fisher Scientific. In addition, the purchase of several fine chemicals from Tokyo Chemical Industry was supported by Soka University, Japan. The chemicals were used directly from the bottles without further purification. The complete list of these chemicals is given in table 2.1.

Table 2.1: List of chemicals used for the syntheses and respective assays

Compound	Assay, %	Company	Assay, %
1,8-Dibromooctane[a]	≥97	1,5-Dibromopentane[b]	97
Aniline[a]	≥99	1,6-Dibromohexane[b]	98
4-Chloroaniline[a]	≥99	1,9-Dibromononane[b]	97
4-Bromoaniline[a]	≥98	1,10-Dibromodecane[b]	97
4-Methylaniline[a]	≥99	1,11-Dibromoundecane[b]	≥98
4-Ethylaniline[a]	≥98	1,12-Dibromododecane[b]	96
1,4-Diaminobenzene[b]	≥99	1,7-Dibromoheptane[c]	97
4-Aminophenol[b]	98	Vanillin[d]	≥98
4-Fluoroaniline[b]	98	Potassium carbonate anhydrous[e]	≥99
4-Hydroxybenzaldehyde[b]	99	Potassium iodide[e]	≥99
2,4-Dihydroxybenzaldehyde[b]	98	4-(4-Hydroxyphenyl)benzoic acid[f]	≥98
2-Thiophenecarbonyl chloride[b]	98	(*RS*)-2-Methyl-1-butanol[f]	≥97
1,4- Dibromobutane[b]	99	(*S*)-(-)-2-Methyl-1-butanol[f]	≥98

[a-f] chemicals obtained from Merck, Acros Organics, Sigma-Aldrich, Fluka, Fisher Scientific and Tokyo Chemical Industry in similar order

2.2 Equipment

Various chemical and physical analyses were conducted to characterize the intermediary and title compounds using instruments which are listed as follow:

1. The melting points of the compounds were determined using Gallenkamp melting point apparatus.
2. The CHN microanalyses were carried out on a Perkin Elmer 2400 LS Series CHNS/O analyzer. The samples were sealed in tin capsules prior to the analyses.
3. The Fourier Transform infrared spectroscopy (FT-IR) analyses were performed on a Perkin Elmer 2000-FTIR spectrometer. The powder samples were mixed homogenously with potassium bromide and subsequently compressed into pellets. The samples were then analyzed in the range of 4000-400 cm^{-1}.
4. The Fourier Transform nuclear magnetic resonance spectroscopy (FT-NMR) analyses were conducted using the Bruker 300 MHz and 400 MHz Ultrashield^{TM} spectrometers. The samples were dissolved in deuterated chloroform containing tetramethylsilane as the internal standard. Due to the partial solubility of several compounds in $CDCl_3$ at room temperature, the spectrometer internal heater was also used to maintain the NMR sample temperature at 55 °C from the point at which the shimming and wobbling was initiated until the scans were completed.
5. The liquid crystalline texture for the compounds were observed using a Carl Zeiss Axioskop 40 polarizing optical microscope equipped with a Linkam TMS94 temperature controller, LTS350 hot-stage and LNP cooling system. For additional optical texture studies, the homeotropic alignment was achieved by coating the microscope slides and glass covers with stearic acid dissolved in chloroform prior to deposition on the surface. The evaporation of chloroform resulted in a thin, transparent film of the stearic acid on the glass surfaces (Dierking, 2003).

6. The thermal properties of the liquid crystals were investigated via differential scanning calorimetry (DSC) and the analyses were carried out using two different instruments as follow:
    i. Seiko DSC120 Model 5500 differential scanning calorimeter at Faculty of Engineering, Soka University, Tokyo, Japan
    ii. Seiko DSC6200R differential scanning calorimeter at Chemical Resources Laboratory, Tokyo Institute of Technology, Yokohama, Japan

   The heating and cooling rates of the Seiko DSC120 Model 5500 and DSC6200R differential scanning calorimeters are ±2 °Cmin^{-1} and ±5 °Cmin^{-1}, respectively. For every series of compounds, only one model of differential scanning calorimeter was used to ensure that the thermal properties of the compounds in that series are comparable to one another.
7. The powder X-ray diffraction analyses were performed on a Bruker D8 diffractometer equipped with a Göbel mirror, Vantec linear detector and vertical goniometer at Department of Chemistry, Warsaw University, Warsaw, Poland. Sample temperature was controlled by Anton Paar heating stage and the θ-θ scans were performed every 0.5 °C.

2.3 Synthesis and characterization

All compounds were synthesized, recrystallized and analyzed at standard atmospheric pressure of 101.325 kPa.

2.3.1 First series

α-(4-Benzylidene-substituted-aniline-4’-oxy)-ω-[2-methylbutyl-4’-(4”-phenyl)-benzoateoxy]alkanes, **4a**-**4j**

The overall synthetic routes towards obtaining α-(4-benzylidene-substituted-aniline-4’-oxy)-ω-[2-methylbutyl-4’-(4”-phenyl)benzoateoxy]alkanes, **4a**-**4j** are shown in figure 2.1. The experimental procedure for every step is given from section 2.3.1.1 to 2.3.1.4.

2.3.1.1 Synthesis of (*RS*)-2-methylbutyl-4’-(4”-hydroxyphenyl)benzoate, **1**

4-(4-Hydroxyphenyl)benzoic acid (1.50 g, 7.0 mmole) was dissolved in 40 mL of (*RS*)-2-methyl-1-butanol in a round-bottom flask. As heat was gradually applied, catalytic amount of concentrated sulphuric acid was added slowly to the stirring mixture and refluxed at 90 °C for 24 h. After reflux, the excess (*RS*)-2-methyl-1-butanol was left at room temperature to evaporate off. The yellow precipitate was recrystallized thrice from the mixture of chloroform and hexane to give the desired white ester.

2.3.1.2 Synthesis of 4-hydroxy-4’-benzylidene-substituted-anilines, **2a**-**2e**

4-Hydroxybenzaldehyde (0.98 g, 8.0 mmole) was dissolved in 40 mL of absolute ethanol in a round-bottom flask. An ethanolic solution of the corresponding aniline (8.0 mmole) was then added dropwise and the mixture was refluxed for 10 h. The resulting solution was left to evaporate off at room temperature. The brown precipitate was subsequently recrystallized from chloroform to yield the desired intermediate categorized as Schiff base. The general molecular formula and amounts of corresponding anilines for the five syntheses are listed accordingly in table 2.2.